Outgassing of ordinary chondritic material and some of its implications for the chemistry of asteroids, planets, and satellites

Laura Schaefer [a,c,*], Bruce Fegley Jr. [a,b,c]

[a] *Planetary Chemistry Laboratory, Washington University, One Brookings Drive, Campus Box 1169, St. Louis, MO 63130-4899, USA*
[b] *McDonnell Center for the Space Sciences, Washington University, One Brookings Drive, Campus Box 1169, St. Louis, MO 63130-4899, USA*
[c] *Department of Earth and Planetary Sciences, Washington University, One Brookings Drive, Campus Box 1169, St. Louis, MO 63130-4899, USA*

Abstract

We used chemical equilibrium calculations to model thermal outgassing of ordinary chondritic material as a function of temperature, pressure, and bulk composition and use our results to discuss outgassing on asteroids and the early Earth. The calculations include ∼1000 solids and gases of the elements Al, C, Ca, Cl, Co, Cr, F, Fe, H, K, Mg, Mn, N, Na, Ni, O, P, S, Si, and Ti. The major outgassed volatiles from ordinary chondritic material are CH_4, H_2, H_2O, N_2, and NH_3 (the latter at conditions where hydrous minerals form). Contrary to widely held assumptions, CO is never the major C-bearing gas during ordinary chondrite metamorphism. The calculated oxygen fugacity (partial pressure) of ordinary chondritic material is close to that of the quartz–fayalite–iron (QFI) buffer. Our results are insensitive to variable total pressure, variable volatile element abundances, and kinetic inhibition of C and N dissolution in Fe metal. Our results predict that Earth's early atmosphere contained CH_4, H_2, H_2O, N_2, and NH_3; similar to that used in Miller—Urey synthesis of organic compounds.
© 2006 Elsevier Inc. All rights reserved.

Keywords: Atmospheres, evolution; Atmospheres, chemistry; Asteroids; Meteorites; Terrestrial planets; Satellites, atmospheres

1. Introduction

The terrestrial planets have secondary atmospheres (Aston, 1924; Russell and Menzel, 1933; Brown, 1949) that originated through the outgassing of volatile-bearing material during and/or after planetary accretion (e.g., see Lange and Ahrens, 1982; Lewis and Prinn, 1984; Abe and Matsui, 1985; Prinn and Fegley, 1987). The outgassed volatiles, which are compounds of H, C, N, O, F, Cl, and S, formed the Earth's early atmosphere and oceans, and the early atmospheres of Mars and Venus. The nature of the early terrestrial atmosphere is of particular interest because it was in this atmospheric environment that the first life forms originated between 4.5 and 3.8 Ga ago (Oró et al., 1990). Whether Mars possessed an early atmosphere conducive for the origin of life is also a matter of intense interest and speculation.

Understanding the nature of Venus' early atmosphere is important for understanding whether Venus once had water and lost it or has been a desert planet throughout its entire history.

Unfortunately, the outgassing of volatiles is a largely unexplored topic that is somewhat like the weather—everyone talks about it, but nobody does anything about it. The only prior study is a Masters thesis by Bukvic (1979) suggested by his advisor J.S. Lewis. Bukvic performed chemical equilibrium calculations for gas–solid equilibria in the upper layers of an Earth-like planet. He modeled the planet's composition using H-chondritic or a mixture of H- and C-chondritic material. From this, he calculated the composition of a volcanically outgassed atmosphere, which he found to be in all cases composed of $CH_4 + H_2$. Bukvic never pursued this work further and it did not attract much attention in the field, despite being discussed by Lewis in Lewis and Prinn (1984).

We decided to model volatile outgassing because it seemed a natural extension of our prior work on vaporization of high temperature lavas and volcanic gas geochemistry on Io (Schae-

* Corresponding author. Fax: +1 (314) 935 7361.
 E-mail addresses: laura_s@wustl.edu (L. Schaefer), bfegley@wustl.edu (B. Fegley).

fer and Fegley, 2004, 2005a, 2005b). The thermal outgassing of volatiles during and after planetary accretion is a question of paramount importance for the origin of planetary atmospheres, thermal metamorphism of meteorites, the chemistry and mineralogy of asteroids, the survival of presolar material in asteroids, satellites, and other bodies, the detection of extrasolar planetary atmospheres, and many other topics.

This paper presents the initial results of our work. We used chemical equilibrium calculations to model the thermal outgassing of ordinary chondritic material, i.e., matter with the average chemical composition of ordinary chondrites. The chondrites are undifferentiated (i.e., unmelted) stony meteorites containing metal + sulfide + silicate. The ordinary (H, L, LL) chondrites constitute about 97% of all chondrites. The chondrites are primitive material from the solar nebula and are generally believed to be the building blocks of the Earth and other rocky asteroids, planets and satellites. Chemical equilibrium calculations predict that ordinary chondritic material was abundant in the inner solar nebula where the terrestrial planets formed (e.g., see Barshay, 1981; Lewis and Prinn, 1984). Geochemical data show that the Earth has a chondritic composition and accreted from a mixture of chondritic materials (e.g., Larimer, 1971; Wänke, 1981; Hart and Zindler, 1986; Kargel and Lewis, 1993; Lodders and Fegley, 1997). For example, the oxygen isotope mixing model predicts that Earth, Mars, and 4 Vesta incorporated ∼21, ∼85, and ∼78% H-chondritic material, respectively (Lodders, 2000). Thus it makes sense to start modeling the outgassing of the most abundant group of chondrites—the ordinary chondrites.

Section 2 describes our computational methods and data. Section 3 describes the results of our calculations and describes the sensitivity of our results to variations in key input parameters. Section 4 discusses some of the applications of our results to asteroids and the primitive Earth. Section 5 summarizes the major points of this paper. We described preliminary results of our work in three abstracts (Fegley and Schaefer, 2006; Schaefer and Fegley, 2005c, 2006).

2. Methods

2.1. Chemical equilibrium calculations

We used chemical equilibrium calculations to model the thermal outgassing of undifferentiated ordinary chondritic material. The chemical equilibrium calculations were done using a Gibbs energy minimization code of the type described by Van Zeggern and Storey (1970). Our calculations consider 20 major rock-forming elements, minor elements, and volatiles in chondrites (Al, C, Ca, Cl, Co, Cr, F, Fe, H, K, Mg, Mn, N, Na, Ni, O, P, S, Si, and Ti). We used the IVTANTHERMO database (Belov et al., 1999), to which we added a number of minerals found in chondrites. In total, our calculations included 224 condensed phases and 704 gaseous species (see Appendix A for a list of condensed phases). Our nominal model uses ideal mineral solid solutions. We also did calculations using pure condensed phases instead of mineral solid solutions and separately considered the effects of C and N dissolution in metal.

2.2. Bulk compositions of ordinary chondrites

We used the average (mean) compositions of H, L and LL chondrites in Table 1 for our nominal models. The H, L, and LL nomenclature refers to the total elemental abundance of iron: high total iron (H, ∼49% of all ordinary chondrites), low total iron (L, ∼36%), and low total iron and low metal (LL, ∼14%). The averages in Table 1 were calculated using compositional data from meteorite *falls*. Falls are meteorites that were observed to fall and were recovered at the time. *Finds* are meteorites, that were found at some later time after they fell on the Earth. There are far fewer falls than finds: only ∼4.5% of all ordinary chondrites are observed falls. Falls are generally less altered or contaminated than finds. Meteorite finds are subjected to contamination and terrestrial weathering, which alters their composition, mineralogy, and volatile element abundances. Terrestrial weathering corrodes metal, adds carbon and water, and increases the Fe^{3+} content of falls (Jarosewich, 1990). For example, the average hydrogen content of H-chondrite finds in the METBASE database (Koblitz, 2005) is over 3 times larger than that of falls. Terrestrial weathering also forms clays, carbonates, sulfates, and rust in meteorite finds.

We calculated the average chondrite compositions in Table 1 from data in the METBASE meteorite database (Koblitz, 2005), using only analyses in which abundances are given for all of the major rock-forming elements (Si, Mg, Fe, Al, Ti, Ca, Na, K, Ni, Co, P, S, Cr, Mn, O). The bulk compositions of average H-, L-, and LL-chondrite falls were calculated from a total of 90, 123, and 29 analyses, respectively. Table 1 also gives the abundance ranges for each constituent (e.g., the range of SiO_2 abundances in the 90 analyses of H chondrites, and so on).

Our results in Table 1 for the average composition of H, L, and LL chondrites are very similar to those reported elsewhere in the literature (e.g., Urey and Craig, 1953; Craig, 1964; Mason, 1965; Jarosewich, 1990). The average values of Urey and Craig (1953) show the biggest discrepancies from our values, but even in this case, the disagreements are relatively minor. The differences arise from several factors including higher quality analyses in recent years, different criteria for including meteorites in an average calculation, meteorite reclassification between the H, L, LL groups since an earlier average was calculated, analyses of new falls, and reporting analytical results with or without volatiles such as water and carbon. We recommend the papers by Urey and Craig (1953) and Mason (1965) for discussion of ordinary chondrite compositions. As described later, we found that compositional variations have only minor effects on our results and do not alter our major conclusions.

2.3. Volatile element speciation and abundances in ordinary chondrites

The ordinary chondrites contain a number of volatile-bearing phases with variable occurrence and abundance. We computed the average values for H, C, N, F, and Cl in Table 1 using data from the METBASE database. The volatile element abundances in meteorites are variable due to intrinsic variations, analytical problems, contamination, and terrestrial weathering.

Table 1
Composition of average ordinary chondrite falls

Component	Mass % of component					
	H chondrite[a]		L chondrite[b]		LL chondrite[c]	
	Range	Average	Range	Average	Range	Average
SiO_2	30.07–39.73	36.49	35.43–42.00	39.66	37.1–41.80	40.48
TiO_2	0.05–0.45	0.12	0.02–0.18	0.12	0.08–0.23	0.13
Al_2O_3	1.46–4.48	2.35	1.35–4.26	2.32	1.84–3.91	2.38
Cr_2O_3	0.10–0.73	0.47	0.05–0.76	0.50	0.36–0.72	0.55
FeO	4.74–17.54	9.54	10.74–17.61	14.14	11.46–21.11	17.44
MnO	0.21–0.50	0.30	0.07–1.21	0.34	0.05–0.45	0.33
MgO	19.77–25.01	23.41	21.11–26.6	24.84	23.81–26.50	25.32
CaO	1.18–2.66	1.70	1.41–2.48	1.84	1.47–2.24	1.82
Na_2O	0.35–1.29	0.87	0.50–2.29	0.98	0.75–1.21	0.96
K_2O	0.04–0.23	0.10	0.03–0.38	0.12	0.05–0.16	0.11
P_2O_5	0.05–0.53	0.26	0.06–0.68	0.25	0.13–0.65	0.27
Fe (m)	8.1–26.19	16.72	2.78–14.68	7.27	0.33–12.93	2.64
Ni	1.15–2.24	1.70	0.70–1.67	1.23	0.73–1.39	1.03
Co	0.01–0.17	0.08	0.01–0.14	0.06	0.02–0.09	0.054
FeS	2.52–9.65	5.33	3.45–9.88	5.99	4.03–8.39	5.87
H_2O^+	0–0.92	0.32	0–1.42	0.34	0–1.77	0.60
H_2O^-	0–0.36	0.09	0–0.36	0.07	0–0.47	0.16
C	0.01–0.34	0.12	0.01–0.90	0.16	0.02–0.57	0.235
N (ppm)	2.05–121	34	4.02–109	34	3–298	50
Cl (ppm)	7–210	77	15–212	76	121–131	126
F (ppm)	8–41	27	8–52	28	49–66	58
Total	–	99.98	–	100.24	–	100.40

[a] No. of analyses: oxides and metals (90), water (47), C (47), N (60), Cl (30), F(7).
[b] No. of analyses: oxides and metals (123), water (84), C (66), N (88), Cl (22), F(11).
[c] No. of analyses: oxides and metals (29), water (18), C (19), N (39), Cl (2), F(3).

It can be difficult to determine whether volatiles are indigenous to a meteorite or arise from terrestrial weathering and/or from handling in museums and elsewhere. This is true for both falls and finds (Consolgmano et al., 1998).

Volatiles (H, C, N) are often extracted from meteorites and isotopically analyzed by multi-step heating at increasingly higher temperatures (e.g., Grady and Wright, 2003; Hashizume and Sugiura, 1997; Yang and Epstein, 1983). The fraction of extracted volatiles with Earth-like isotopic compositions is often dismissed as terrestrial contamination. For our considerations here, however, we assume that all volatiles measured for a particular meteorite are indigenous. We do this because there is no guarantee that some of the low temperature "contaminants" are not actually indigenous. This may make our nominal model more volatile-rich than a pristine ordinary chondrite. However, thermal metamorphism on meteorite parent bodies has altered the chondrites now in our meteorite collections. Originally, chondritic material was plausibly even more volatile-rich than even the most volatile-rich ordinary chondrite samples in meteorite collections today. The larger volatile abundances in the unequilibrated ordinary chondrites (i.e., the H3, L3, LL3 chondrites), which are less metamorphically altered than the grade 4–6 ordinary chondrites, support this argument.

To mitigate the effect of taking a volatile-rich nominal model, we have done sensitivity studies on the effects of volatile abundances on our results. We varied the abundances of H, C, O, N, and S over the ranges observed in ordinary chondrites. We describe these results in a later section. We also did calculations using individual analyses of some falls (e.g., Bruderheim

L6, Chainpur LL3.4, Homestead L5, New Concord L6) in the METBASE database and noticed no significant difference in our results between the individuals and the average compositions.

2.3.1. Hydrogen

Hydrogen occurs as organic compounds and water (absorbed, hydrated salts, hydrous silicates). Kaplan (1971) asserted that there is no indigenous hydrogen in any chondrites except carbonaceous chondrites. However, the subsequent discovery of deuterium-rich material in ordinary chondrites (Robert et al., 1979; McNaughton et al., 1981; Yang and Epstein, 1983) shows that at least some of the hydrogen in ordinary chondrites is indigenous. Recently, Menzies et al. (2005) used X-ray diffraction and Mössbauer spectroscopy to detect phyllosilicates in unequilibrated ordinary chondrites. The discovery of fluid inclusions and halite in the Monahans (1998) and Zag H chondrites also shows that indigenous water existed on ordinary chondrite parent bodies (Rubin et al., 2002, and references therein). Table 1 lists H_2O instead of H because most meteorite chemical analyses list H_2O^- (water minus) and H_2O^+ (water plus). The H_2O^- is water released by drying at $110\,°C$ and is loosely bound hydrogen such as physically absorbed water and some of the water in hydrated salts and clays. The H_2O^+ is water released by heating at high temperatures and is fixed hydrogen such as H in organic matter, OH in minerals, and more strongly bound water in hydrated minerals (Breger and Chandler, 1969).

Our average values for water in H, L, and LL chondrites (see Table 1) agree with those ($H_2O^+ = 0.32\%$ for H, 0.37% for L, and 0.51% for LL chondrites) from Jarosewich (1990). In contrast, H_2O values from multi-step heating and isotopic analyses of ordinary chondrites range from 0.01–0.34% and are somewhat lower than our average values (Robert et al., 1979, 1987a, 1987b; McNaughton et al., 1981, 1982; Yang and Epstein, 1983).

2.3.2. Carbon

Carbon occurs as graphite, poorly graphitized carbon, carbides, C dissolved in Fe alloy, organic material, and diamonds. Our average values for the carbon abundances in ordinary chondrites generally agree with those from other sources. Table 1 gives 0.12% (range = 0.01–0.34%), Jarosewich (1990) gives $0.11 \pm 0.18\%$, Vdovykin and Moore (1971) give 0.11% (range = 0.02–0.35%), and Grady and Wright (2003) give a range of 0.03–0.60% for ordinary (H, L, LL) chondrites.

2.3.3. Nitrogen

Nitrogen occurs as organic matter, nitrides, N dissolved in Fe alloy, and possibly as ammonium salts (reviewed in Fegley, 1983). The small amounts of nitrogen in ordinary chondrites ($\sim$2–120 ppm = μg/g) are difficult to extract due to its inertness (Kung and Clayton, 1978). We used nitrogen data from METBASE and other sources (Hashizume and Sugiura, 1992, 1995, 1997; Sugiura et al., 1996, 1998; Gibson and Moore, 1972a; Moore and Gibson, 1969; Kothari and Goel, 1974). Jarosewich (1990) does not give values for nitrogen. Our average (mean) values (in ppm = μg/g) are 34 (H), 34 (L), and 50 (LL). These are slightly lower than the median values (also in ppm = μg/g) of 48 (H), 43 (L), and 70 (LL) from Mason (1979).

2.3.4. Fluorine and chlorine

These elements occur in apatite $Ca_5(PO_4)_3(OH, F, Cl)$ and occasionally as halide salts. Apatite can account for all of the chlorine in chondrites, but only a fraction of the fluorine, of which most must be present in other phases (Mason, 1979). The halogens are difficult to analyze (Mason 1971, 1979; Dreibus et al., 1979), and older analyses give higher values than actually present. We used F and Cl analyses from METBASE, Allen and Clark (1977), Dreibus et al. (1979), and Garrison et al. (2000). Mason (1979) gives average values (in ppm = μg/g) of 32 (H), 41 (L), and 63 (LL) for fluorine, slightly higher than our average values in Table 1. Our average values for chlorine are virtually identical to those in Mason (1979).

2.4. Temperature–pressure profiles of ordinary chondrite parent bodies

We did most of our calculations using temperature–pressure (T–P) profiles for the asteroid 6 Hebe to model the outgassing of ordinary chondritic material. We also studied the effects of variable total pressure at constant temperature and of variable temperature at constant total pressure on our results. Gaffey and Gilbert (1998) argue that 6 Hebe is a prime candidate
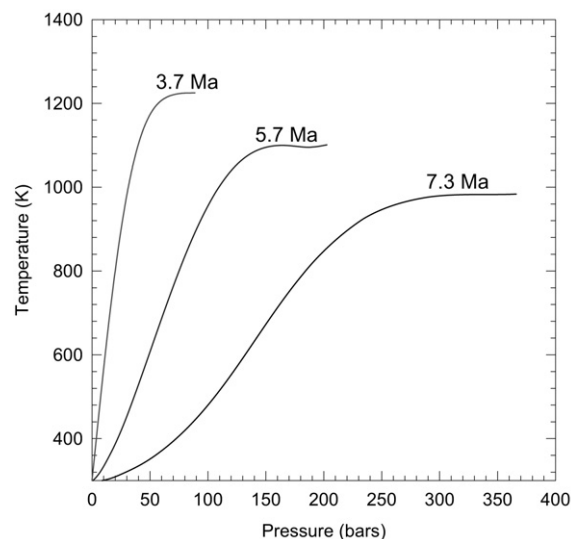

Fig. 1. Pressure vs temperature profiles for Asteroid 6 Hebe based on the temperature vs depth profiles from Ghosh et al. (2003). The different lines refer to temperature profiles at 3.7, 5.7, and 7.3 Ma after accretion.

for the H-chondrite parent body based on its spectral slope and orbit. Ghosh et al. (2003) developed a thermal model for Asteroid 6 Hebe, taking into account both radioactive and accretionary heating. They calculated temperature versus depth profiles for the asteroid at various time intervals since the beginning of accretion (3.7, 5.7, and 7.3 Ma after accretion) and assumed a peak metamorphic temperature of 1225 K (McSween et al., 1988). A recent study (Slater-Reynolds and McSween, 2005) places the peak metamorphic temperature for H chondrites slightly lower at 1200 K. However, the difference in our calculated results for a peak temperature of 1200 K is insignificant, so we used the temperature–depth profiles of Ghosh et al. (2003) to calculate the T–P profiles shown in Fig. 1. Using hydrostatic equilibrium, we calculated the lithostatic pressure for the bulk density of Hebe (3.7 ± 1.2 g/cm^3) measured by Michalak (2001). We calculated g for a body of the total radius at 3.7, 5.7, and 7.3 Ma after accretion. We did not consider the variation of g with depth. For our nominal model, we used the 3.7 Ma T–P profile shown in Fig. 1. All figures hereafter use this T–P profile unless otherwise stated. If we had used the average H chondrite density of 3.4 g/cm^3 (Britt and Consolmagno, 2003) we would calculate slightly lower pressures at a given depth. However, as discussed in Section 3.3, slightly lower (or higher) pressures at a given temperature do not significantly change our conclusions.

We used the ideal gas law and average volatile element abundances to see if using the lithostatic pressure as the total gas pressure is sensible. We did a calculation assuming that all carbon in an average H chondrite is in the gas and used $\rho = 3.4$ g/cm^3 and porosity = 10% (Britt and Consolmagno, 2003). This gives $P_{gas} \sim 340$ bars within the pore spaces at 1200 K, the maximum metamorphic temperature for an H6 chondrite (Slater-Reynolds and McSween, 2005). If we assume all hydrogen in an average H chondrite is present as H_2 gas (as our results show), P_{gas} increases to $\sim$1120 bars. This exceeds

the calculated pressure of ~400 bars at the center of 6 Hebe and would break it apart.

Wilson et al. (1999) did a detailed study of internal gas pressures in asteroidal bodies. They found that closed systems typically generate internal gas pressures of tens to thousands of bars, sometimes sufficient to cause explosive disruption of the body. Open systems with extensive fracturing near the surface lose gases to space more efficiently, so the greatest internal gas pressures are found near the center of the body. The calculations of Wilson et al. (1999) were done for carbonaceous chondrites; ordinary chondrites should generate smaller but still substantial pressures. For the sake of this paper, we consider our meteorite parent bodies to be closed systems and assume that

$$P_{gas} = P_{lithostatic}. \tag{1}$$

In addition to the above arguments in favor of such large gas pressures, we note that Eq. (1) is a common assumption in terrestrial metamorphic studies (see, for instance, Spear, 1995). We discuss the effect of total pressure and of open vs closed systems on our results in Sections 3.3 and 3.4.

The maximum temperature we used in our calculations is 1225 K, from the asteroid thermal modeling of Ghosh et al. (2003). This temperature is set by the fact that there is no observed eutectic melting in type 6 ordinary chondrites. Takahashi (1983) melted a Yamato L3 chondrite at pressures from 6 to 30 kbar and found a solidus of 1225 K, defined by the Fe–Ni–S eutectic regardless of pressure for an oxygen fugacity (i.e., partial pressure) equal to the iron–wüstite (IW) buffer. They found the silicate solidus to be ~250 K higher. Since our calculations are set by the thermal model for Hebe ($T < 1225$ K), we are always below the solidus.

2.5. Comparison to meteorite heating experiments

In order to test our calculations, we searched the literature for experiments involving heating of ordinary chondrites and analyses of the gas released. We found remarkably few relevant papers on this subject. Most work on heating and evolved gas analysis was done using carbonaceous chondrites, but these are not the subject of this paper. A number of studies were performed around the turn of the 19th/20th century until the 1920s or so (e.g., Travers, 1898, 1899; Merrill, 1926; Nash and Baxter, 1947; Ansdell and Dewar, 1886). In principle, these experiments could be useful, but in practice, we cannot use them for comparisons. One reason is that the exact temperature of heating is typically unknown. Samples are described as being heated to a "dull red heat," which may correspond to temperatures between 600–900 °C. Another reason is that the collected gases are cooled before being analyzed. The cooling probably changes the equilibrium composition of the gas and removes condensable species, such as water vapor, before analysis. Finally, many of the meteorites analyzed are iron meteorites, rather than stony meteorites.

Experiments during the Apollo era looked at gases implanted and trapped in lunar samples (e.g., Gibson and Moore, 1972b; Gibson and Johnson, 1971; Müller, 1972; Funkhouser et al., 1971). However, gases trapped inside rocks are different
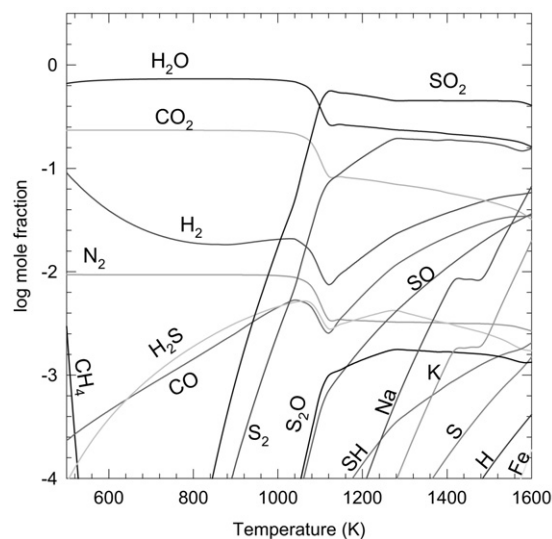

Fig. 2. The chemical equilibrium gas composition as a function of temperature for the Holbrook (L6) meteorite at a total pressure of 10^{-3} bar.

than gases evolved from volatile-bearing phases during heating. Also, the lunar samples are closer to basaltic achondrites than to chondrites.

The most relevant work is that of Gooding and Muenow (1977). They heated a sample of the Holbrook meteorite, an L6 chondrite fall which was recovered in 1912. The heating was done under vacuum in a stepwise fashion; that is, as gas evolved from the chondrite, it was removed and the temperature was gradually increased. Therefore, their experiment is for an open system with evolving bulk composition. We calculated the equilibrium gas chemistry using a bulk chemical analysis of the Holbrook chondrite from Gibson and Bogard (1978). Our results are for a closed system with a constant bulk composition, but are qualitatively similar to those of Gooding and Muenow (1977). They found that H_2O and CO_2 were the primary hydrogen and carbon bearing species, with S_2 and minor amounts of SO_2 becoming abundant above 1073 K. Our results (Fig. 2) show that H_2O and CO_2 are the most abundant gases below ~1050 K. From 1050 K to higher temperatures SO_2, H_2O, and S_2 are the three most abundant gases in this order. The equilibrium calculations do not agree with the heating experiment at high temperatures because of the nature of the stepwise heating experiment. By removing the gases released at lower temperatures, primarily H_2O and CO_2, the heated Holbrook sample became more reducing and chemical equilibrium shifted from SO_2 to S_2.

Muenow et al. (1995) heated several ordinary chondrites in a vacuum and measured the gases that were evolved. They found that H_2O and CH_4 outgassed below ~900 K. Carbon dioxide formed around 1023 K, and CO was released from ~1100–1300 K. Our results indicate that H_2 is the most abundant gas, although Muenow et al. (1995) do not mention measuring any H_2. We also find that CH_4 is only abundant below ~600 K. Above this temperature we find that CO is more abundant than CO_2, and H_2 is more abundant than H_2O. However, due to the experimental set up used by Muenow et al. (1995) and their rapid heating rate, it is unclear that equilibrium is achieved in
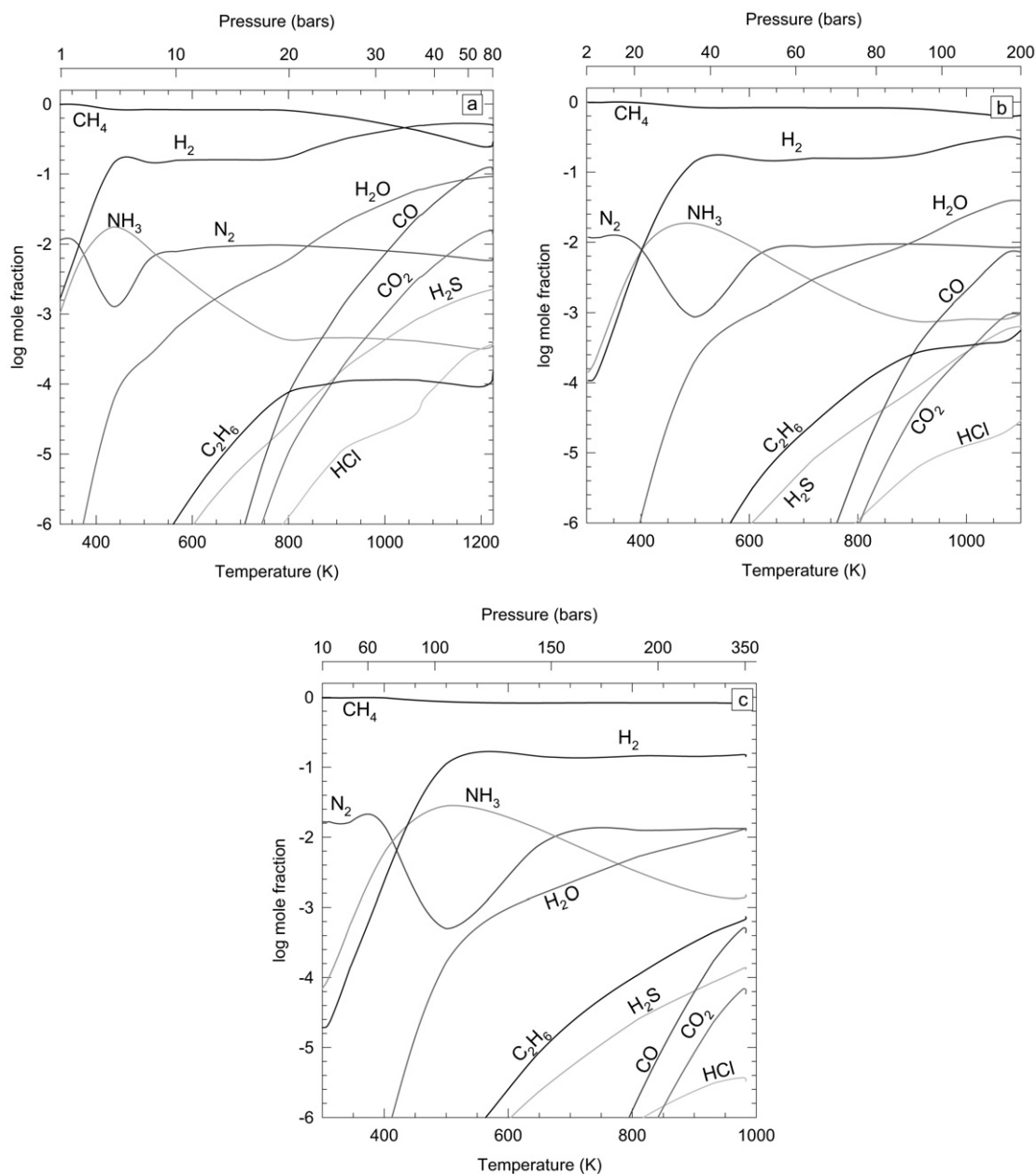
Fig. 3. Chemical equilibrium composition of volatiles outgassed from average H-chondritic material as a function of temperature for three different $T-P$ profiles for the Asteroid 6 Hebe: (a) 3.7, (b) 5.7, (c) 7.3 Ma after accretion. The thermal profiles are given in Fig. 1.

their system. This is further supported by the fact that their heating experiment did not release all of the volatiles; for instance, their measured abundance of C for the Sharps (H3.4) chondrite was only ∼21% of the total carbon abundance as given in the literature (see Table 1 of Muenow et al., 1995).

3. Results

3.1. Nominal model—gas chemistry

Fig. 3 shows the calculated gas composition for average H-chondritic material along the three temperature–pressure profiles shown in Fig. 1. The temperatures correspond to depth within the parent body, with the coldest temperature at the surface, and the highest temperature at the center of the body. Fig. 3a shows the calculated gas composition of average H-chondritic material for the 3.7 Ma Hebe temperature–pressure profile. The major gas at low temperatures is CH_4. The abundance of methane begins to drop at ∼800 K when graphite becomes a stable solid phase. At ∼1050 K, H_2 becomes the most abundant gas. Water vapor is always less abundant than H_2. Nitrogen is primarily found in N_2, with lesser amounts of NH_3. The brief peak in NH_3 abundance at ∼450 K is caused by the decomposition of talc, which releases more hydrogen into the gas phase. However, H_2 and H_2O rapidly steal hydrogen away from NH_3 as temperature increases. CO and CO_2 become more abundant at higher temperatures but are never more abundant than methane. CO is the third most abundant gas at high tem-
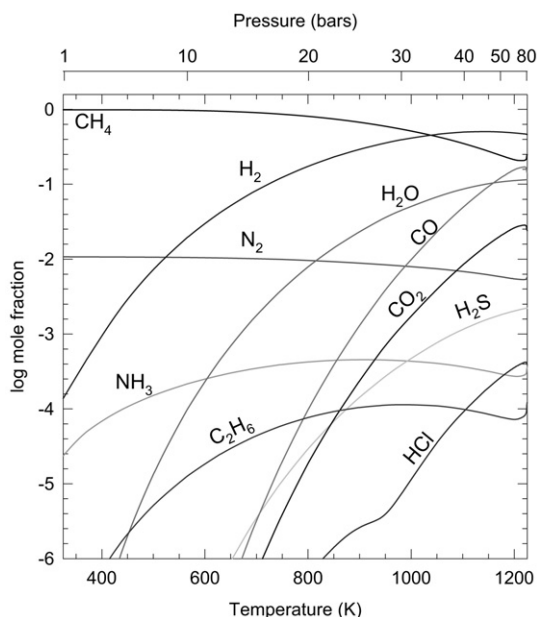
Fig. 4. Chemical equilibrium composition of volatiles outgassed from average L-chondritic material as a function of temperature. The 3.7 Ma thermal profile for the Asteroid 6 Hebe is used for the calculations.
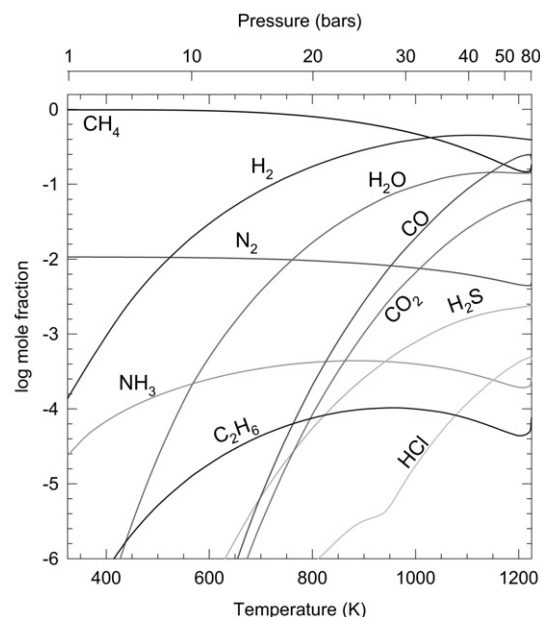

Fig. 5. Chemical equilibrium composition of volatiles outgassed from average LL-chondritic material as a function of temperature. The 3.7 Ma thermal profile for the Asteroid 6 Hebe is used for the calculations.

peratures and is always more abundant than CO_2. All gaseous sulfur, chlorine, and fluorine are found in H_2S, HCl, and HF (off scale at lower abundances), respectively.

Figs. 4 and 5 are the analogs to Fig. 3a for average L- and LL-chondritic material, respectively. The gas compositions for all ordinary chondritic material are very similar with only minor differences. The small peak in the ammonia abundance observed in H-chondritic material is missing in L- and LL-chondritic material. The associated plateau in the H_2 (g) abundance seen in H chondrites is also missing for L and LL chondrites. The differences exist because talc is not stable in our calculations for L- and LL-chondritic material but is stable in H-chondritic material. Talc forms in H- but not L- and LL-chondritic material because the calculated water vapor partial pressure in the latter two cases is lower than that needed for talc formation. In turn, the lower water vapor partial pressures are due to the higher carbon contents of L- and LL-chondritic material which lead to more CH_4 and less H_2O than in H-chondritic material. (We discuss observations of talc and other hydrous silicates in ordinary chondrites in Sections 2.3 and 3.2.) The CH_4/H_2 crossover point is almost identical for all three types of ordinary chondritic material. Carbon monoxide and CO_2 are more abundant (and CH_4 less abundant) at high temperatures for both L- and LL-chondrites than for H-chondrites. For LL-chondritic material, CO becomes the second most abundant gas above ∼1175 K, and CH_4 and H_2O are about equally abundant.

Fig. 3b shows the calculated gas composition for H-chondritic material using the 5.7 Ma Hebe temperature–pressure profile. In Fig. 3b, CH_4 remains the most abundant gas at all temperatures. The slight decrease in CH_4 (and associated increase in H_2) above ∼900 K is due to the formation of graphite. Talc is present to slightly higher temperatures (∼500 K), which causes the broadening of the NH_3 peak. Fig. 3c shows the gas

composition for H-chondritic material gas along the 7.3 Ma Hebe T–P profile. Methane gas is again the most abundant species. Diatomic hydrogen is the second most abundant gas above ∼400 K. Water vapor is less abundant than N_2 gas at all temperatures. Ammonia is more abundant than N_2 gas from 400–650 K, at which temperature talc decomposes. Carbon monoxide and CO_2 are less abundant than C_2H_6.

We do not show the analogous figures for the 5.7 Ma and 7.3 Ma T–P profiles for L- or LL-chondritic material given the close similarities in gas chemistry with H-chondritic material. As before, the major differences between the types of ordinary chondritic material are that the peak in the ammonia abundances and the plateau of the H_2 and H_2O abundances seen in H-chondrites are missing from the L and LL chondrites.

Fig. 6 shows the distribution of the volatile elements (H, C, O, and S) between the major gas and solid species for the calculations shown in Fig. 3a. All nitrogen is in the gas; we discuss its solubility in metal in Section 3.6. Fig. 6a shows the distribution of hydrogen between the major H-bearing gases (CH_4, C_2H_6, H_2, H_2O, H_2S, HCl, NH_3) and the solid phases talc $Mg_3Si_4O_{10}(OH)_2$ and hydroxyapatite $Ca_5(PO_4)_3OH$. Note the logarithmic abundance scale in Fig. 6a. The major H-bearing species are CH_4, H_2, and, at low temperatures, talc. Fig. 6b shows the distribution of carbon between the major C-bearing gases (CH_4, CO, and CO_2) and graphite. At equilibrium, CH_4 is the major carbon-bearing species at all temperatures. (The fact that any carbon remains in chondrites shows they are disequilibrium assemblages.) We consider the effect of C dissolution in metal in Section 3.6. Fig. 6c shows the distribution of oxygen between solid phases (silicates and oxides, see Section 3.2) and the major gases H_2O, CO, and CO_2. The amount of oxygen found in the gas phase is insignificant at low temperatures and is less than 0.3% of total oxygen at the highest temperatures.
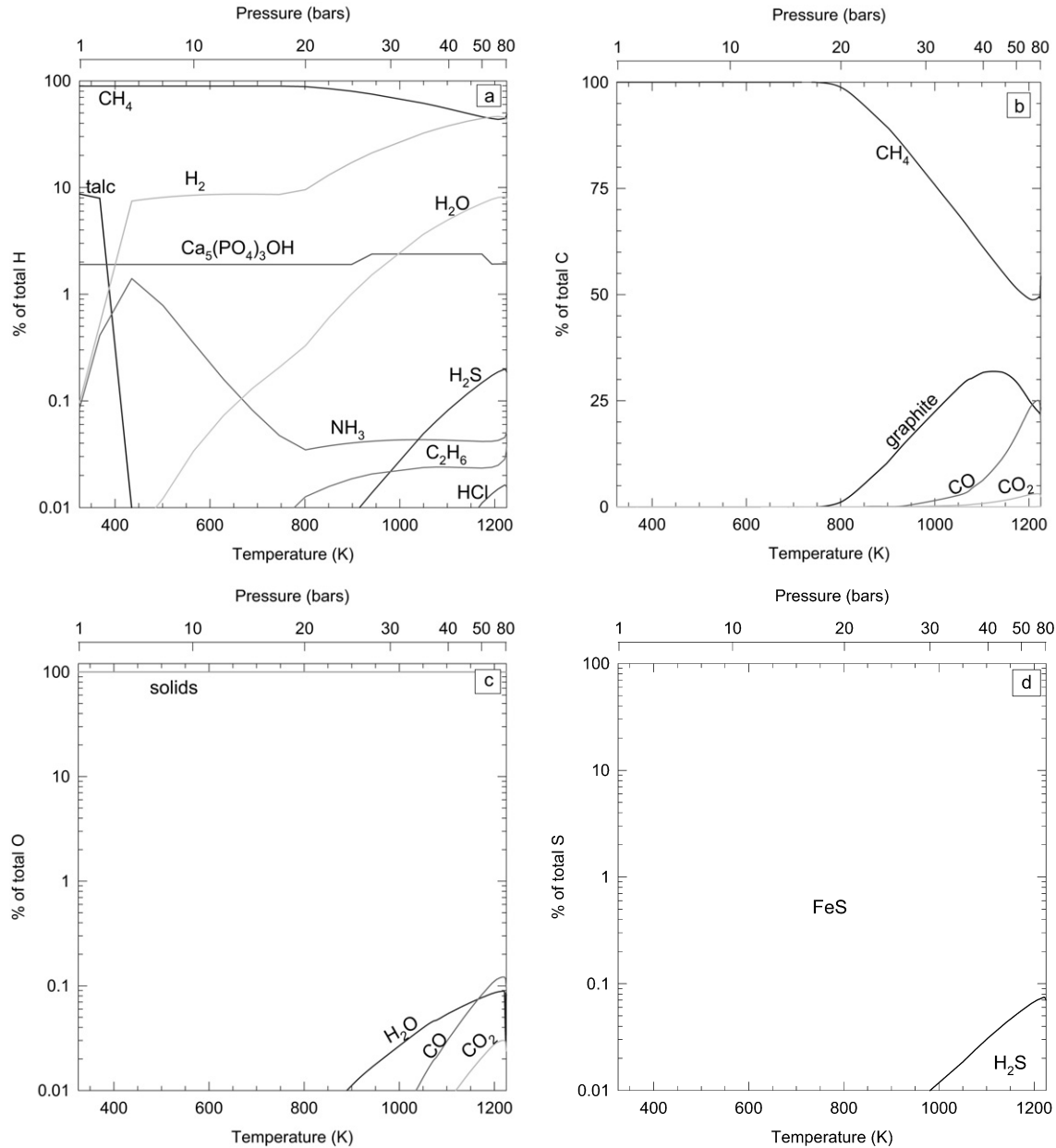
Fig. 6. Chemical equilibrium distribution of volatile elements between the major solid and gas phases for average H-chondritic material. Calculations use the Hebe 3.7 Ma thermal profile. Results are expressed as percentage of each element as a function of temperature: (a) hydrogen, (b) carbon, (c) oxygen, (d) sulfur.

Fig. 6d shows the distribution of sulfur between troilite (FeS) and the gas phase (H_2S). The amount of sulfur in the gas is insignificant (<0.1%) at all temperatures. As long as both Fe metal and troilite are present the total amount of sulfur in the gas is regulated by the iron-troilite sulfur fugacity buffer. The equation and S_2 fugacity for this buffer are (Fegley and Osborne, 2006)

$$FeS \text{ (troilite)} = Fe \text{ (metal)} + \frac{1}{2}S_2 \text{ (g)}, \qquad (2)$$
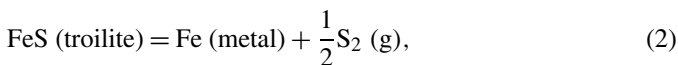
$$\log f_{S_2}(\text{bar}) = 13.7393 - \frac{17,308}{T} - 2.2007\log T$$
$$+ \frac{0.1160(P - 1)}{T}. \qquad (3)$$

For example, at our highest T–P point along the 3.7 Ma thermal profile (1225 K, 88.8 bars) the sulfur fugacity $fS_2 \sim 6.4 \times 10^{-8}$ bar for reaction (2). The reaction of H_2 with this S_2 vapor controls the equilibrium partial pressure of H_2S.

Fig. 7a shows the regions in T/P space in which CH_4, CO, and graphite are the most abundant C-bearing compounds within H-chondritic material. The solid lines are equal abundance lines. The dotted line continues the CH_4/CO equal abundance line within the graphite-dominant field. The shaded region represents the temperatures and pressures for the three thermal profiles of 6 Hebe (see Fig. 1). As shown in Fig. 7a, methane is always the most abundant C-bearing gas along our nominal T–P profile. The tip of the shaded area closest to the CH_4/CO boundary is the peak temperature (1225 K). It is en-
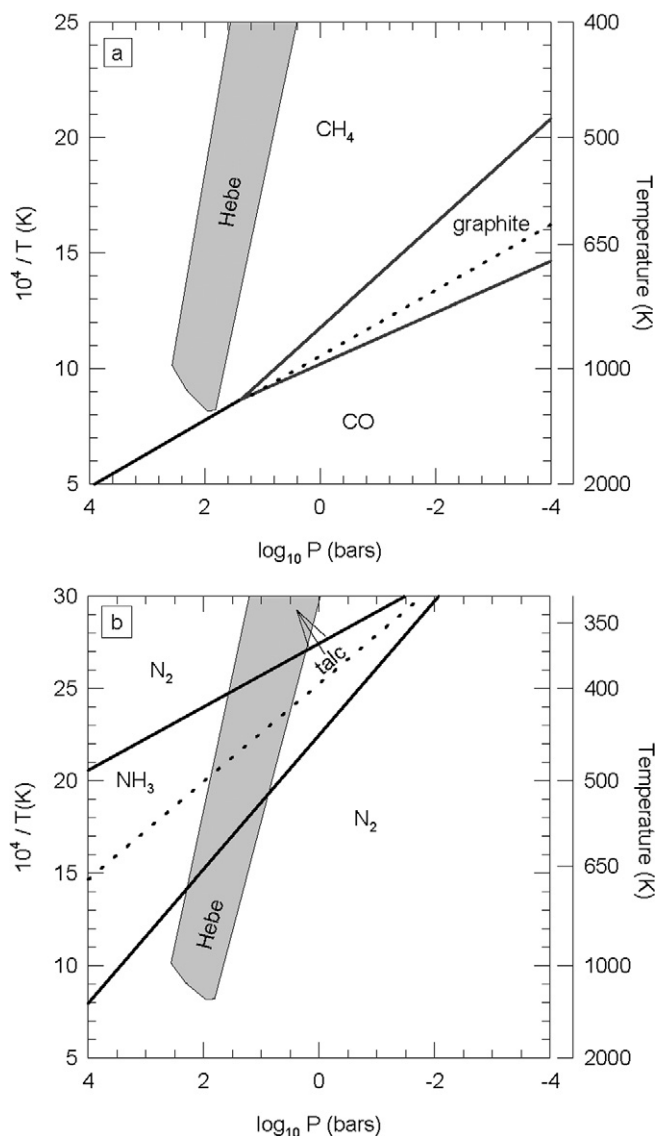
Fig. 7. (a) The chemical equilibrium distribution of carbon between CH_4, CO, and graphite for average H-chondritic material plotted as a function of temperature and pressure. The solid lines are equal abundance lines showing where $CH_4/CO = 1$, $CH_4/graphite = 1$, and $graphite/CO = 1$. The dashed line is the extension of the CH_4/CO equal abundance line into the field where graphite is dominant. (b) The chemical equilibrium distribution of nitrogen between N_2 and NH_3 for average H-chondritic material plotted as a function of temperature and pressure. The solid lines are equal abundance lines showing where $N_2 = NH_3$. The region where $NH_3 > N_2$ is smaller for L- and LL-chondritic material. The dotted line shows where talc (in average H-chondritic material) or chlorapatite (in average L- and LL-chondritic material) is stable. The shaded region in both plots is the T–P range in thermal models for Asteroid 6 Hebe (see Fig. 1).

tirely plausible that, for a slightly different accretion scenario in which the peak temperature is reached at shallower depths (lower pressures), 6 Hebe lies at least partially within the CO stability field. However, over time, the asteroid would evolve into the CH_4 field (assuming a closed system).

We made similar calculations for average L- and LL-chondritic material. Our results show that 1:1 contours in L- and LL-chondritic material move to slightly lower temperatures (at a given pressure) than for H-chondritic material. Assuming the

same T–P profile as for 6 Hebe, the L-chondrite parent body is always within the CH_4 field. However, the LL-chondrite parent body lies marginally within the CO field.

Fig. 7b shows the equal abundance lines for N_2/NH_3 for average H-chondritic material. Ammonia is more abundant than N_2 in a small region of T–P space that partially overlaps the T–P profiles used for 6 Hebe. The abundance of NH_3 in H-chondritic material seems to be tied to the presence of talc $(Mg_3Si_4O_{10}(OH)_2)$, shown with a dotted line. Talc is stable above this line at low temperatures and high pressures. However, this is not true for L- and LL-chondritic material. We found no conditions under which ammonia was more abundant than N_2 for L- or LL-chondritic material.

Fig. 8 shows the calculated oxygen fugacities (fO_2) for average H-, L-, and LL-chondritic material as a function of temperature compared to some common oxygen fugacity buffers and measurements of oxygen fugacities of heated meteorite samples. (The figure caption explains the abbreviations for the different oxygen fugacity buffers.) The oxygen fugacity of average H-chondritic material (Fig. 8a) lies slightly below the quartz-fayalite-iron (QFI) buffer, and the oxygen fugacity of average L-chondritic material (Fig. 8b) lies directly on the QFI buffer. O'Neill (1987) electrochemically measured the oxygen fugacity of the QFI buffer from 900–1400 K

$$Fe_2SiO_4 \text{ (fayalite)} = 2Fe \text{ (metal)} + SiO_2 \text{ (quartz)}$$
$$+ O_2(g). \tag{4}$$
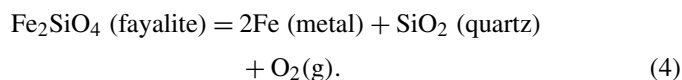
His results are represented by the equation (Fegley and Osborne, 2006)

$$\log f_{O_2}(\text{bar}) = 4.5468 - \frac{29{,}194}{T} + 0.8868 \log T$$
$$+ \frac{0.0497(P-1)}{T}. \tag{5}$$

The fayalite and metal involved in this buffer in ordinary chondritic material are present in solid solution and are not present as pure phases. Pure quartz is not present but the coexistence of olivine and pyroxene buffers the SiO_2 activity at a given temperature. The oxygen fugacity of average LL-chondritic material (Fig. 8c) is slightly larger than that of L-chondritic material and lies slightly above the QFI buffer. It is reasonable to expect that the oxygen fugacity of ordinary chondritic material should be near the QFI buffer.

Brett and Sato (1984) measured the intrinsic oxygen fugacities of two H, one L, and two LL chondrites. They found that H-chondrites were more reduced than L and LL chondrites, and that the oxygen fugacities of the five ordinary chondrites measured were within a narrow range less than 0.7 log units wide. The points on the graphs show their results. Our calculated oxygen fugacities agree very well with their results. An abstract by Walter and Doan (1969) reports intrinsic oxygen fugacities of one H and one L chondrite. For the H chondrite, their measurements are significantly lower than those of Brett and Sato (1984) and our calculated fugacities. Their measured fugacities for the L chondrite Holbrook agree better with, but are still lower than, the data of Brett and Sato (1984). McSween and
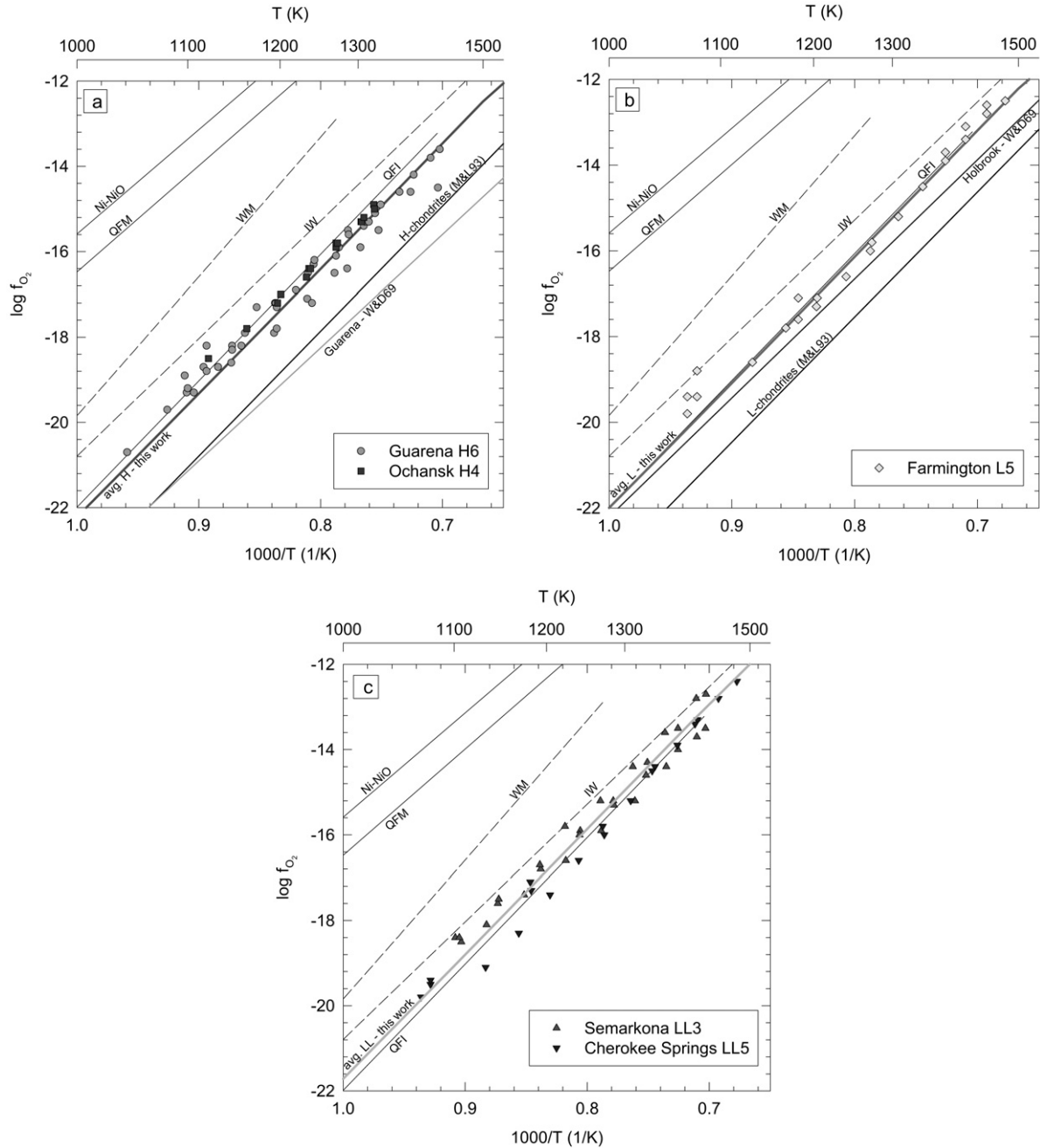
Fig. 8. (a) The chemical equilibrium oxygen fugacity of average H-chondritic material as a function of temperature compared to different solid-state oxygen fugacity buffers. The points are intrinsic oxygen fugacities of the Guareña (H6) and Ochansk (H4) chondrites measured by Brett and Sato (1984). Also shown are the intrinsic oxygen fugacities of the Guareña (H6) chondrite measured by Walter and Doan (1969) and the calculated oxygen fugacities for average H4–H6 chondrites from McSween and Labotka (1993). (b) The chemical equilibrium oxygen fugacity of average L-chondritic material as a function of temperature compared to different solid-state oxygen fugacity buffers. The points are intrinsic oxygen fugacities of the Farmington (L5) chondrite measured by Brett and Sato (1984). Also shown are the intrinsic oxygen fugacities of the Holbrook (L6) chondrite measured by Walter and Doan (1969) and the calculated oxygen fugacities for average L4–L6 chondrites from McSween and Labotka (1993). (c) The chemical equilibrium oxygen fugacity of average LL-chondritic material as a function of temperature compared to different solid-state oxygen fugacity buffers. The points are intrinsic oxygen fugacities of the Semarkona (LL3) and Cherokee Springs (LL5) chondrites measured by Brett and Sato (1984). (IW = iron–wüstite, QFI = quartz–fayalite–iron, QFM = quartz–fayalite–magnetite, WM = wüstite–magnetite).

Labotka (1993) calculated oxygen fugacities for average H4–H6 and L4–L6 chondrites from the compositions of coexisting olivine, orthopyroxene, and metal using the fayalite–ferrosilite–iron (FFI) oxygen fugacity buffer

$$2Fe_2SiO_4 \text{ (fayalite)} = 2FeSiO_3 \text{ (ferrosilite)} + 2Fe \text{ (metal)}$$
$$+ O_2 \text{ (g)}. \qquad (6)$$
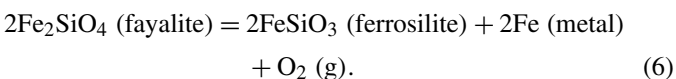
(The lines shown on the graphs are extrapolations of their data to higher temperatures.) Calculated oxygen fugacities from McSween and Labotka (1993) are lower than the measured values of Brett and Sato (1984) and our calculated fO₂ values. Their results for H chondrites agree at lower temperatures with the oxygen fugacities for one H chondrite measured by Walter and Doan (1969).

The fO$_2$ of the FFI buffer cannot be measured and must be calculated from thermodynamic data because ferrosilite is thermodynamically unstable at low pressures. At 1200 K our calculated fO$_2$ for reaction (6) is about 1.4 log fO$_2$ units higher (i.e., more oxidizing) than that of McSween and Labotka (1993). The difference is apparently due to the thermodynamic data they used for the FFI buffer. Traditionally the FFI buffer is used to define the fO$_2$ of ordinary chondrites because olivine, pyroxene, and iron alloy are three abundant phases in these meteorites. However, the difficulty with this approach is that different groups use different thermodynamic data for the FFI buffer and get different results for the oxygen fugacity of ordinary chondrites. For example, at 1200 K Brett and Sato (1984) measured $\log fO_2$ (bars) $= -17.1 \pm 0.6$ for the Ochansk H4 chondrite and -17.3 ± 0.6 for the Guareňa H6 chondrite. At the same temperature we calculate $\log fO_2 = -17.4 \pm 0.4$ for H chondritic material, Williams (1971) calculated -17.5 ± 1.2, and McSween and Labotka (1993) calculated -18.8 for $\log fO_2$.

3.2. Nominal model—Mineralogy

The major minerals found in ordinary chondrites are: olivine (Mg,Fe)$_2$SiO$_4$, Ca-poor pyroxene (Mg,Fe)SiO$_3$, plagioclase (Na,K,Ca)(Al,Si)$_4$O$_8$, diopside CaMgSi$_2$O$_6$, chromite FeCr$_2$O$_4$, chlorapatite Ca$_5$(PO$_4$)$_3$Cl and/or whitlockite Ca$_9$MgH(PO$_4$)$_7$, kamacite α-(Fe,Ni), taenite γ-(Fe,Ni), and troilite FeS (Rubin, 1997). The abundances of Fe-bearing silicates increase from H to L to LL chondrites whereas the abundance of metal decreases from H to LL. Carbides are rare and occur primarily as cohenite (Fe$_3$C) in unequilibrated ordinary chondrites (Krot et al., 1997). However, the distribution of carbon between carbides, graphite, organic matter, diamond, and other phases in ordinary chondrites is generally unknown.

Our calculated compositions contain all of the above minerals with the exception of whitlockite. We also found talc Mg$_3$Si$_4$O$_{10}$(OH)$_2$, which is a phyllosilicate, and graphite to be stable. Talc typically occurs in meteorites as a terrestrial weathering product. However, phyllosilicates occur in the Bishunpur and Semarkona unequilibrated ordinary chondrites (Hutchison et al., 1987; Alexander et al., 1989; Keller, 1998). Brearley (1997) observed talc in the Allende CV3 chondrite, and Rietmeijer and Mackinnon (1985) observed talc in a chondritic interplanetary dust particle. Menzies et al. (2005) found phyllosilicates in unequilibrated H, L, and LL chondrites by X-ray diffraction and Mössbauer spectroscopy. Graphite and poorly graphitized carbon occur in ordinary chondrites (Ramdohr, 1973; Grady and Wright, 2003; Mostefaoui et al., 2005), but are uncommon. Ramdohr (1973) reports that the graphite in the Grady H3 chondrite "resembles that produced by the thermal decomposition of hydrocarbons in retorts and coke ovens, and must have been produced under comparable conditions."

Fig. 9 shows the calculated mineralogy of average H chondritic material for the 3.7 Ma Hebe T–P profile. These calculations included ideal solid solutions for olivine (Mg,Fe,Mn)$_2$-SiO$_4$, orthopyroxene (Mg,Fe,Ca,Mn)SiO$_3$, metal (Fe,Ni,Co), and feldspar (Na,K,Ca)(Al,Si)$_4$O$_8$. We did not model clinopy-
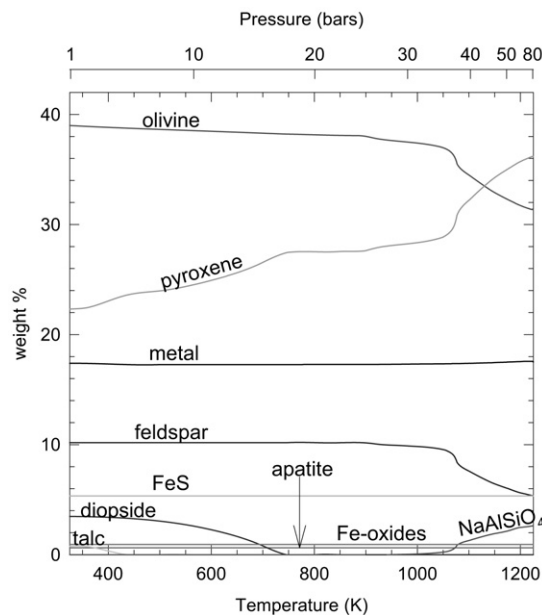

Fig. 9. The mineralogy of average H-chondritic material plotted as a function of temperature and pressure along the Hebe 3.7 Ma thermal profile. The calculations assume ideal solid solutions.

Table 2
Solid solution compositions

Solid solution	Observed	Hebe (3.7 Ma)[a]
	H chondrites	
Olivine	Fo$_{80-84}$Fa$_{20-16}$	Fo$_{77-86}$Fa$_{23-14}$
Ca-poor pyroxene[b]	En$_{86-80}$Fs$_{14-20}$	En$_{83-67}$Fs$_{17-28}$Wo$_{0-5}$
Plagioclase	An$_{12}$Ab$_{82}$Or$_6$	An$_{21-39}$Ab$_{73-50}$Or$_{6-11}$
	L chondrites	
Olivine	Fo$_{75-79}$Fa$_{25-21}$	Fo$_{71-80}$Fa$_{29-20}$
Ca-poor pyroxene[b]	En$_{81-78}$Fs$_{19-22}$	En$_{79-60}$Fs$_{19-31}$Wo$_{0-9}$
Plagioclase	An$_{10}$Ab$_{84}$Or$_6$	An$_{14-40}$Ab$_{79-42}$Or$_{6-18}$
	LL chondrites	
Olivine	Fo$_{68-74}$Fa$_{32-26}$	Fo$_{67-75}$Fa$_{33-25}$
Ca-poor pyroxene[b]	En$_{78-74}$Fs$_{22-26}$	En$_{77-56}$Fs$_{21-34}$Wo$_{0-9}$
Plagioclase	An$_{10}$Ab$_{86}$Or$_4$	An$_{17-47}$Ab$_{77-38}$Or$_{6-16}$

[a] Calculated solid solution composition for the 3.7 Ma Hebe T/P profile from low T to high T (e.g., olv = Fo$_{77}$Fa$_{23}$ @ 300 K, olv = Fo$_{86}$Fa$_{14}$ @ 1225 K for H chondrites).

[b] For calculated compositions, remainder is found in MnSiO$_3$.

roxene solid solutions but included pure diopside CaMgSi$_2$O$_6$, hedenbergite CaFeSi$_2$O$_6$, and acmite NaFeSi$_2$O$_6$ in our calculations. Minor phases that are stable but not abundant enough to be visible in Fig. 9 are talc ($T < 500$ K), graphite ($T > 800$ K), and sodalite (950–1175 K). The Fe-oxides include chromite (FeCr$_2$O$_4$) and ilmenite (FeTiO$_3$).

Table 2 gives the compositions of the olivine, pyroxene, and feldspar solid solutions. Our calculated olivine compositions for average H- and L-chondritic material are more fayalitic at lower temperatures and more forsteritic at higher temperatures than observed in H and L chondrites. Olivine compositions for average LL-chondritic material match the observed values in LL chondrites. Our calculated pyroxene compositions match observations well at lower temperatures but are too Fe and Ca-rich at higher temperatures. There is no temperature at which we can match both olivine and pyroxene compositions simulta-

Table 3
Normative mineralogy of ordinary chondrites compared with calculated mineralogies

Mineral (mass %)	Avg. H chondrite[a]	Hebe (3.7 Ma)[b]
Apatite	0.65 ± 0.07	0.62
Chromite	0.76 ± 0.05	0.70
Ilmenite	0.23 ± 0.02	0.23
Orthoclase	0.56 ± 0.07	0.60
Albite	7.30 ± 0.31	7.33–2.72
Anorthite	1.70 ± 0.43	2.22–2.27
Diopside	4.11 ± 0.54	3.48–0
Hypersthene	26.15 ± 2.94	22.18–35.63
Olivine	35.04 ± 3.93	39.10–31.90
Metal	18.02 ± 1.65	17.36–16.78
FeS	5.47 ± 0.38	4.96
Total	99.99	98.78–96.41[c]

Mineral (wt%)	Avg. L chondrite[a]	Hebe (3.7 Ma)[b]
Apatite	0.54 ± 0.09	0.59
Chromite	0.78 ± 0.05	0.74
Ilmenite	0.24 ± 0.02	0.23
Orthoclase	0.64 ± 0.07	0.71
Albite	8.07 ± 0.44	8.29–1.51
Anorthite	1.59 ± 0.49	1.58–1.55
Diopside	4.97 ± 0.66	4.59–0
Hypersthene	24.15 ± 2.59	20.66–38.44
Olivine	44.83 ± 3.02	49.32–38.39
Metal	8.39 ± 0.99	7.30–6.59
FeS	5.80 ± 0.80	5.99
Total	100.00	100.00–92.64[c]

Mineral (wt%)	Avg. LL chondrite[a]	Hebe (3.7 Ma)[b]
Apatite	0.54 ± 0.11	0.64
Chromite	0.80 ± 0.04	0.81
Ilmenite	0.25 ± 0.04	0.25
Orthoclase	0.61 ± 0.12	0.65
Albite	8.11 ± 0.50	8.13–1.45
Anorthite	1.55 ± 0.40	1.86–1.91
Diopside	5.34 ± 0.54	4.19–0
Hypersthene	21.44 ± 3.73	17.10–35.83
Olivine	51.92 ± 5.57	58.60–46.04
Metal	3.59 ± 1.65	1.60–2.41
FeS	5.85 ± 1.06	5.16–5.89
Total	100.00	98.99–95.88[c]

[a] From McSween et al. (1991).
[b] Calculated for the 3.7 Ma Hebe T/P profile. Ranges are from low to high T (300–1225 K).
[c] Other phases present: H: corundum, talc, Fe_2C, MnS, sodalite, nepheline; L: C, Fe_2C, sodalite, nepheline; LL: C, Fe_2C, sodalite, nepheline, Ni_3S_2.

neously for any of the ordinary chondrites. Our feldspar compositions are too Ca-rich at all temperatures, especially at high temperatures. At high temperatures, albite transforms into sodalite $Na_8Al_6Si_6O_{24}Cl_2$ and nepheline $NaAlSiO_4$.

Table 3 compares the normative mineralogies for average ordinary chondrites from McSween et al. (1991) with our calculated mineralogies. We find that there is good overlap between our calculated mineralogies and the normative mineralogies. The amounts of minor phases such as apatite, chromite, and ilmenite are essentially identical, although apatite is slightly higher than the norm in LL chondrites. For the feldspathic constituents, we have good agreement with the orthoclase abundance at all temperatures. Our albite abundance at lower tem-

peratures agrees with the normative albite abundance; however, as temperature increases, our albite abundance decreases and becomes significantly lower than the normative abundance. Our anorthite abundance does not change significantly with temperature. It is slightly higher than the normative anorthite abundance for H and LL chondrites, but agrees well for L chondrites. Our calculated abundances of orthopyroxene solid solution increase with temperature and match the normative hypersthene value at ~700 K for H- and L-chondrites and ~750 K for LL chondrites. However, the calculated pyroxene compositions at these temperatures are significantly more Fe-rich than the observed values listed in Table 2. Our olivine abundance decreases with temperature and matches the normative value at ~1100 K for H chondrites, ~1000 K for L chondrites, and ~1020 K for LL chondrites. The olivine compositions at these temperatures fall within the observed range of compositions listed in Table 2. Our calculated metal abundances decrease slightly with temperature and are somewhat lower than the normative metal abundances. Our calculated troilite abundance is approximately constant with temperature for H and L chondrites and increases with temperature for LL chondrites.

Two factors are probably responsible for the differences between our calculated olivine and pyroxene compositions and those observed in H, L, and LL chondrites. The first factor is that ordinary chondrites are not equilibrium assemblages. The terms "equilibrated chondrites" and "un-equilibrated chondrites" do not denote chemical equilibrium or a lack thereof. Instead, the term "equilibrated chondrites" refers to the homogeneity of FeO content in olivines and pyroxenes. Unequilibrated chondrites have a broad range of FeO contents in olivine and pyroxene, whereas equilibrated chondrites have a narrow range of FeO contents. The second factor is the sensitivity of Fe–Mg exchange between olivine and pyroxene to very small changes in the Gibbs energies of forsterite, fayalite, enstatite, and ferrosilite. The Fe–Mg exchange reaction is

$$\frac{1}{2}Fe_2SiO_4 + MgSiO_3 = FeSiO_3 + \frac{1}{2}Mg_2SiO_4. \qquad (7)$$
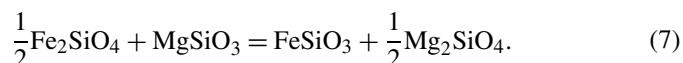
The standard Gibbs energy change $\Delta_r G^o$ for this reaction is only a few hundred to few thousand joules and is about the same size as the uncertainties in the thermodynamic data. For example, using data from the compilation of Robie and Hemingway (1995) $\Delta_r G^o = 2000 \, J\,mol^{-1}$ at 800 K. For comparison, Robie and Hemingway (1995) list uncertainties of ± 1300 (fayalite), ± 1600 (enstatite), ± 3000 (ferrosilite), and ± 2000 (forsterite) $J\,mol^{-1}$ on the Gibbs energies at 298 K. Von Seckendorff and O'Neill (1993) also commented on the sensitivity of Fe–Mg exchange between olivine and pyroxene. Their comparison of experimental partitioning data shows significant disagreement between different experimental data sets.

If we artificially set both the olivine and orthopyroxene compositions to the average values observed in H chondrites, we match the normative mineralogy almost exactly. The greatest deviations from the norms is the metal abundance (16.8– 17.9 mass%), which is again slightly less than the average observed value (Table 3), but still within the range of values observed.
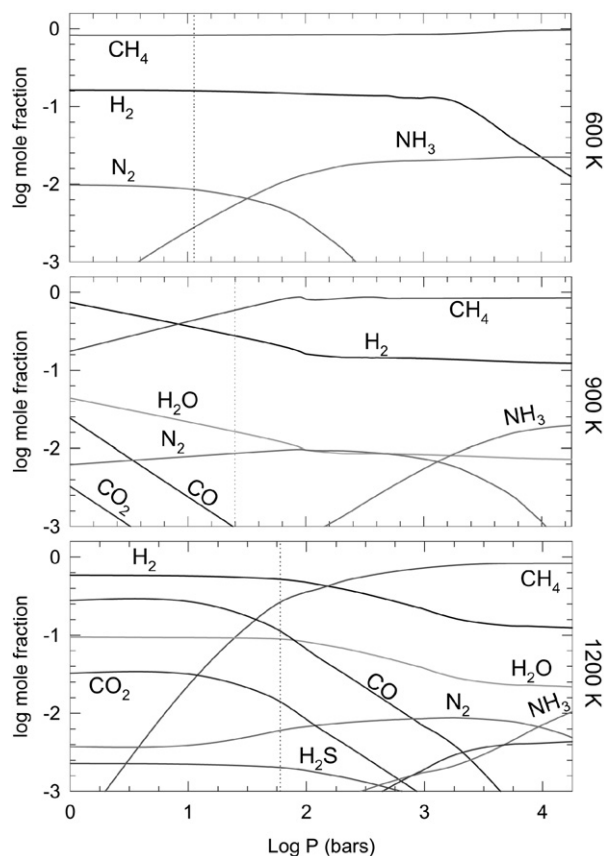
Fig. 10. The equilibrium gas chemistry of average H-chondritic material plotted as a function of pressure at constant temperatures of 600, 900, and 1200 K. Dashed lines indicate the total pressure of the nominal model at each temperature.

Fig. 11. The chemical equilibrium oxygen fugacity of average H-chondritic material as a function of temperature for pressures of 1–10,000 bars.

3.3. Effect of variable total pressure

As we stated earlier, we assumed that the total gas pressure is equal to the lithostatic or confining pressure. However, the gas pressure could be greater or less than the lithostatic pressure in other situations. For instance, an impact into a planetesimal's surface could cause fracturing, which would allow gas to escape from the interior, lowering the pressure. Also, asteroids should have a small but finite permeability, especially smaller asteroids, which have significant macroporosity and therefore act as open systems. This allows gas to escape from the interior and reduces the internal gas pressure. We therefore decided to look at the effect of total pressure on the calculated gas chemistry.

Fig. 10 shows the calculated gas chemistry for average H chondritic material as a function of pressure at constant temperatures of 600, 900, and 1200 K. Note the logarithmic scale for the total pressure. At all three temperatures, H_2 and CH_4 are the most abundant gases. H_2 is the most abundant gas at low pressures and high temperatures, whereas methane is the most abundant gas at low temperatures and high pressures. As we discussed earlier, the CH_4/H_2 crossover point occurs at higher pressures at higher temperatures (see the 900 and 1200 K panels). The abundance of water vapor decreases with increasing pressure and then levels off (see the 900 and 1200 K panels). The H_2O abundance also decreases slightly with increasing
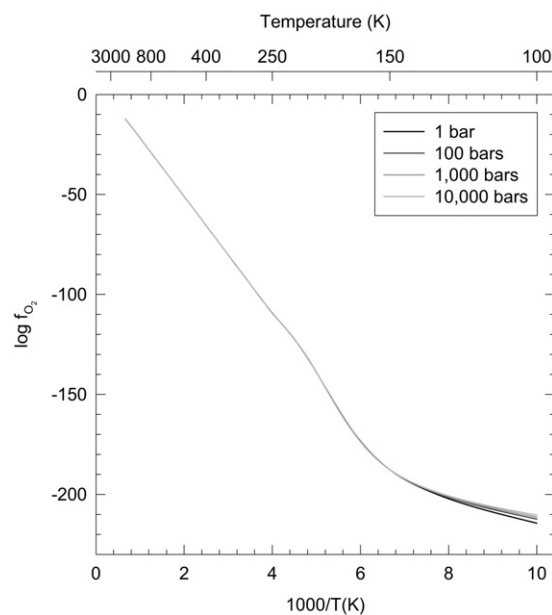
temperature (compare the 900 and 1200 K panels). Carbon monoxide and CO_2 become abundant gases at high temperatures and low pressures (1200 K panel). The CH_4/CO intersection at 1200 K in Fig. 10 corresponds to the position of the 1:1 CH_4/CO contour in Fig. 7a. Ammonia and N_2 are less abundant at higher temperatures because there are more volatiles in the gas phase. We found similar results for average L- and LL-chondritic material.

Fig. 11 shows the calculated oxygen fugacity for average H-chondritic material as a function of temperature at pressures ranging from 1 bar to 10 kbars. As can be seen in the figure, the oxygen fugacity is independent of pressure at temperatures greater than 150 K. This is expected when a solid-state buffer controls the oxygen fugacity because of the relatively small volume change between the different solid phases involved in the buffer (e.g., see Eq. (5) for the QFI buffer).

3.4. Closed system vs open system

An open system reduces the total internal gas pressure and allows volatiles to escape, which alters the bulk composition of the system. As stated above, many asteroids, especially small ones, have significant macroporosity and function as open systems. It is therefore important for us to look at the effect of volatile loss on our calculations. To simulate an open system, we did a series of calculations in which we moved outgassed material from deeper layers upwards, re-equilibrated the volatiles within the next higher layer, and moved the outgassed volatiles upwards again. In this way, we transported essentially all volatiles from the interior of the parent body to its surface. Fig. 12 shows the gas composition for our open system calculation. The major gas is H_2 at all levels, followed by CH_4, H_2O, and NH_3. The mineralogy at the lower levels is essentially the same as in the closed system. In the layers
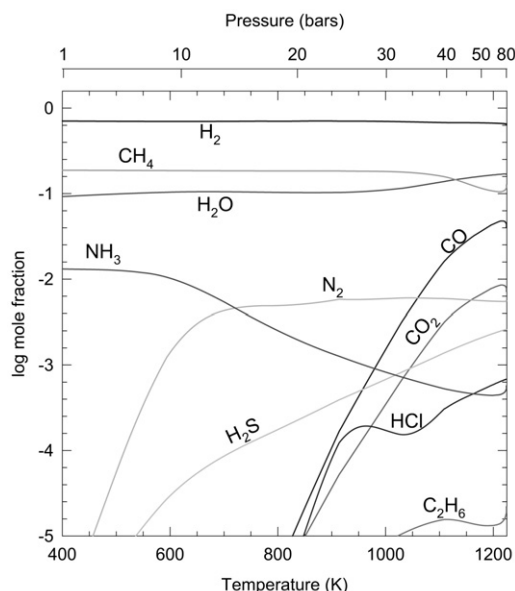
Fig. 12. The equilibrium gas chemistry plotted as a function of temperature for average H-chondritic material in an open system. Calculations are done using the 3.7 Ma Hebe thermal profile.

near the surface, the mineralogy changes and spinel $MgAl_2O_4$, magnetite Fe_3O_4, and muscovite $KAl_3Si_3O_{10}(OH)_2$ are stable.

3.5. Effect of volatile element abundances on gas chemistry

As we discussed earlier, the volatile contents of meteorites may be significantly affected by terrestrial contamination. In order to understand the effect of volatile content on the gas chemistry, we did calculations for the entire range of volatile contents measured in the ordinary chondrites. We did this by using the average H chondrite abundances given in Table 1 and substituting a different abundance for one of the volatiles (H, C, N, O, and S) at a time. The ranges of volatile abundances used are given in Table 1. All calculations are done using the 3.7 Ma thermal profile in Fig. 1. Our results are given in Figs. 13–16 and are discussed below.

3.5.1. Hydrogen

Fig. 13 illustrates the effect of H abundance on gas chemistry. We found no difference whether we varied hydrogen as pure H or as H_2O. The top panel of Fig. 13 shows the gas chemistry for a hydrogen abundance of 2.8 mg/g (2.5% H_2O) with all other elemental abundances being those given in Table 1. With this large hydrogen abundance, H_2 becomes the most abundant gas at all temperatures and pressures. The second most abundant gases are CH_4 below ∼900 K and H_2O at higher temperatures. Methane is always more abundant than CO. The second panel is our nominal model (see Fig. 3a). In the third panel, the hydrogen abundance is 0.01 mg/g (0.0089% H_2O). There is significantly less matter in the gas phase, such that N_2 gas becomes the most abundant gas. The second most abundant gases are CH_4 and H_2. Methane is more abundant at temperatures below ∼850 K, and H_2 is more abundant at
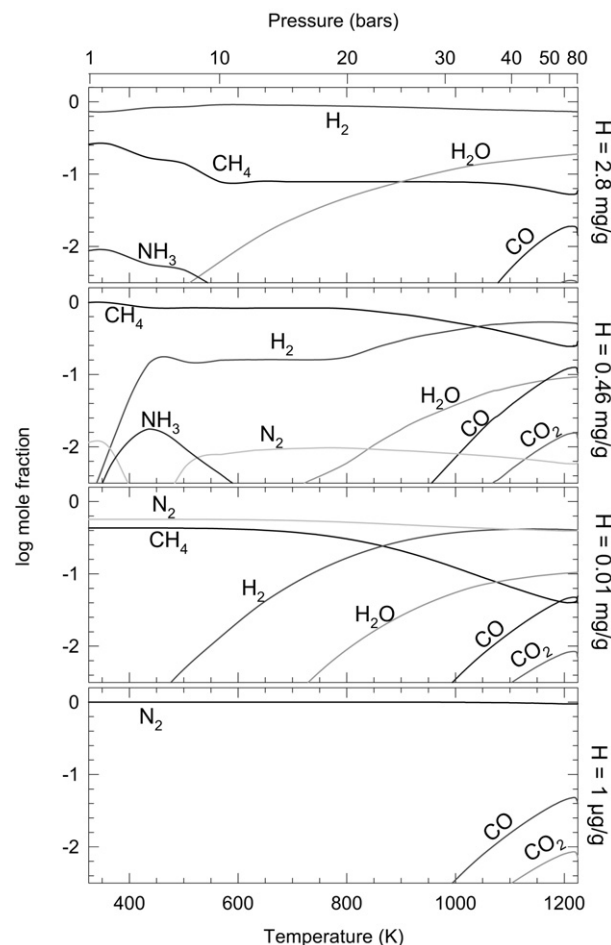

Fig. 13. Equilibrium gas chemistry as a function of temperature and hydrogen elemental abundance for average H-chondritic material: (a) H = 2.8 mg/g (2.5% H_2O), (b) H = 0.46 mg/g (0.41% H_2O nominal value), (c) H = 0.01 mg/g (0.0089% H_2O), (d) H = 1 µg/g (8.9 µg/g H_2O). Calculations are done using the 3.7 Ma Hebe thermal profile.

higher temperatures. Water vapor is also fairly abundant and becomes more abundant than CH_4 above ∼1050 K. Methane is more abundant than CO until ∼1200 K, above which CO is more abundant. The bottom panel shows the gas chemistry for an H abundance of 1 µg/g (8.9 µg/g H_2O), which is less than the smallest measured abundance of H in ordinary chondrites. We did this computation to determine what happens if Kaplan's assertion that all hydrogen in ordinary chondrites is due to terrestrial contamination is correct. For this computation, most carbon is in graphite. Therefore, the only significantly abundant gas is N_2, with minor amounts of CO and CO_2 at high temperatures.

3.5.2. Carbon

Fig. 14 shows the effect of C abundance on gas chemistry. The top panel of Fig. 14 shows the gas chemistry for a carbon abundance of 3.4 mg/g (0.34% C). The gas chemistry is very similar to the average case, shown in the middle panel. The major difference is that, in the higher C case, the H_2 abundance does not level out between 500–850 K, and there is no peak of NH_3 gas, similar to the behavior of volatiles out-
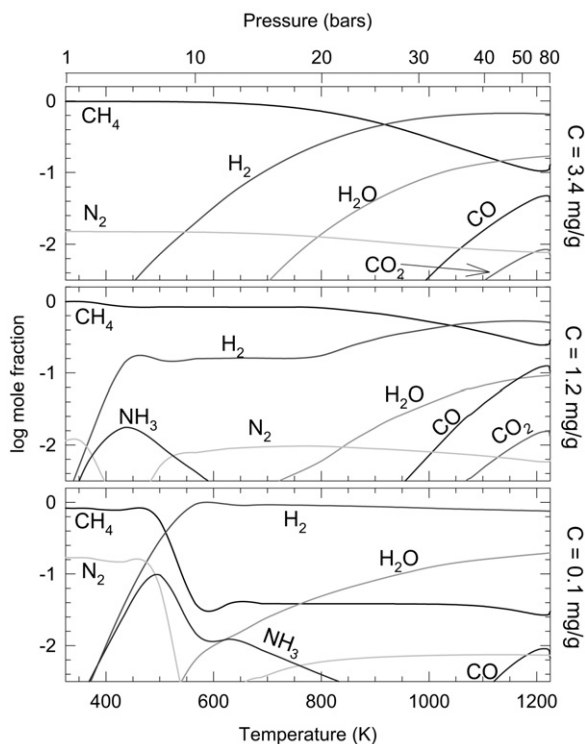
Fig. 14. Equilibrium gas chemistry as a function of temperature and carbon elemental abundance for average H-chondritic material: (a) C = 3.4 mg/g, (b) C = 1.2 mg/g (nominal value), (c) C = 0.1 mg/g. Calculations are done using the 3.7 Ma Hebe thermal profile.

Fig. 15. Equilibrium gas chemistry as a function of temperature and nitrogen elemental abundance for average H-chondritic material: (a) N = 121 ppm, (b) N = 34 ppm (nominal value), (c) N = 5 ppm. Calculations are done using the 3.7 Ma Hebe thermal profile.

gassed from average L-chondritic material (Fig. 4). In the average case, the sudden rise and plateau of the H_2 abundance is caused by the decomposition of talc, but in the high C case, talc is never stable, so we do not see the same effect. The gas abundances at higher temperatures are essentially identical, including the CH_4/H_2 cross-over point. The bottom panel of Fig. 14 shows the gas chemistry for a carbon abundance of 0.1 mg/g (0.01% C). Below ∼500 K, the most abundant gases are CH_4 and N_2. Above this temperature, talc decomposes, and H_2 becomes the most abundant gas. Methane remains the second most abundant gas until ∼750 K, when H_2O becomes more abundant. Nitrogen gas converts into ammonia at ∼500 K, and both fall off in abundance at higher temperatures. Carbon monoxide is never significantly abundant.

3.5.3. Nitrogen

Table 1 gives a range of nitrogen contents for H chondrites of 2–121 ppm (=µg/g). Using this range, we examined the effect of varying nitrogen composition on the bulk gas chemistry (Fig. 15). The middle panel in this plot is the nominal case. Changing the nitrogen abundance only changes the abundances of the major N-bearing gases and has no effect on the other major gases, such as CH_4, H_2, and H_2O. For the higher N abundance, N_2 is more abundant, and ammonia does not become more abundant than N_2, even at the point of talc decomposition. For the low N abundance, both N_2 and NH_3 are less abundant, and are off scale the bottom of the graph.
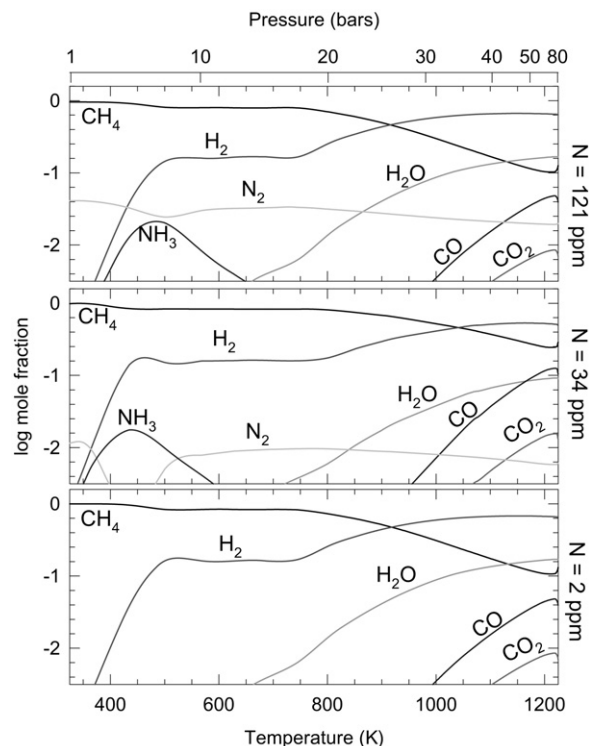
3.5.4. Oxygen

Fig. 16 shows the variation of gas chemistry with oxygen abundance. Oxygen abundances found in H chondrites range from 27.7% (Rose City H5 chondrite) to 37.2% (Conquista H4 chondrite). The mean and median oxygen elemental abundances in H chondrites are essentially identical and are 33.55%.

The reported oxygen abundance of 27.7 wt% for the Rose City meteorite (Mason and Wiik, 1966) is probably much lower than the actual oxygen abundance. Rose City is a brecciated and veined meteorite (Fig. 5 of Mason and Wiik, 1966) and it is difficult to get a representative sample for chemical analysis without consuming a large amount of the meteorite. The average oxygen abundance in high iron enstatite (EH) chondrite falls is 28.7 wt% with a range of 27.6–29.3 wt%. It is unreasonable that the more oxidized Rose City ordinary chondrite would have a smaller oxygen abundance than EH chondrites. However, excluding Rose City from the calculations does not significantly alter the mean and median oxygen abundance of H chondrites.

Oxygen is typically not determined directly, but rather by difference after all other elements have been measured. Most H-chondrites have oxygen abundances within the range 32–36 wt%. Within this range, there is no significant difference in gas chemistry, as can be seen in the second and third panels of Fig. 16. There are only a few meteorites with oxygen abundances outside this range. For H chondrites with larger oxygen abundances, up to 38 wt%, the abundances of NH_3, CO, and
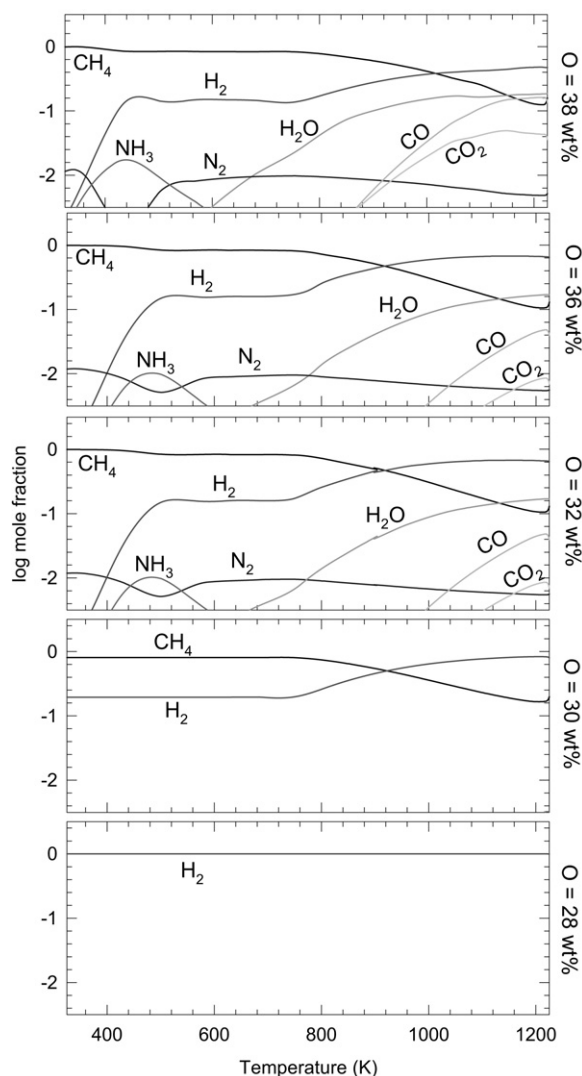
Fig. 16. Equilibrium gas chemistry as a function of temperature and oxygen elemental abundance for average H-chondritic material: (a) O = 38 wt%, (b) O = 36 wt%, (c) O = 32 wt%, (d) O = 30 wt%, (e) O = 28 wt%. Calculations are done using the 3.7 Ma Hebe thermal profile.

CO_2 increase and the CH_4/H_2 crossover point shifts to a slightly higher temperature ($\sim$1000 K). At lower oxygen abundances, the gas phase chemistry changes drastically, as can be see in the bottom two panels of Fig. 16. The solid phase chemistry also changes dramatically. For these cases, there is insufficient oxygen available to form silicates. Instead, normally lithophile elements form sulfides (CaS, MgS, CrS and TiS), schreibersite (Fe_3P), silicides (Cr_2Si, $TiSi_2$), Si metal, SiC, and sinoite (Si_2N_2O). These phases are not typically found in ordinary chondrites but are often found in enstatite chondrites and achondrites.

3.5.5. Sulfur

We used the range of sulfur abundances (8.2–35.2 mg/g) to check if the sulfur abundance had any effect upon the gas chemistry, as we have done above with hydrogen and carbon. The abundances of the stable solid phases changed somewhat, primarily troilite and iron metal. For the low sulfur abundance,

troilite was less abundant and iron metal was consequently more abundant, and the reverse for the high sulfur abundance. The major gas phase chemistry is identical for all sulfur abundances.

3.6. Solubility of carbon and nitrogen in metal

As mentioned in Section 2.3, carbon and nitrogen are often found dissolved in chondritic metal. We included graphite, Fe_2C, Fe_3C (cohenite or cementite), and Fe_4N (roaldite) in our nominal model. We found that Fe_4N was never a stable phase, which indicates to first approximation that nitrogen dissolution in metal should be minor. Nitrogen dissolves in metal as monatomic N and we calculated its solubility using data from Chipman and Elliott (1963) as described in Fegley (1983). We assumed that all nitrogen is found in either N_2 (g) or is dissolved in metal, which is a valid assumption at high temperatures. At low temperatures, the solubility of N in metal is negligible. At higher temperatures, we found that the amount of nitrogen dissolved in metal increases, but is still well within the variability of the total nitrogen content of ordinary chondrites.

Fig. 17a shows the results of our calculations. Using the average nitrogen abundance of 34 ppm (=µg/g) in H chondrites, we found that $\sim$24% of total nitrogen ($\sim$8 ppm) is dissolved in Fe metal at 1225 K. This leaves $\sim$26 ppm nitrogen in the gas. With decreasing temperature, the amount of dissolved nitrogen decreases and becomes insignificant ($<$1% of total nitrogen) below 900 K. Using a more sophisticated solution model, Hashizume and Sugiura (1998) found 5–30 ppm (=µg/g) of N dissolved in taenite (γ-Fe,Ni), regardless of the initial nitrogen concentration, which agrees well with our result. Our sensitivity calculations, where all nitrogen was found in the gas, showed that there was little effect on gas chemistry for nitrogen abundances of 2–121 ppm.

Solubility of carbon in metal is more important for our applications because the abundance of carbon in the gas phase is more important for determining the major gas chemistry. It is also consequently a much more difficult problem because carbon occurs in many more compounds than nitrogen. In our nominal model, we found that graphite is stable at high temperatures. We used data on γ-Fe–C alloys from Richardson (1953) to calculate the approximate effect of carbon solubility on our system. (Richardson's data are very similar to those of Chipman (1972) but are in a more convenient form to use.) As with nitrogen, we found large amounts of carbon dissolved in Fe at high temperatures, decreasing with temperature. Results are shown in Fig. 17b. At 1225 K, we found $\sim$5000 ppm (0.5%) C in Fe metal ($\sim$65% of total carbon). This concentration drops to $\sim$500 ppm (0.05% C) by 800 K, and $\sim$1 ppm (10^{-4}% C) by 600 K. There was no appreciable amount of C in metal at lower temperatures. No iron carbides were stable when carbon dissolved in Fe. Our calculated concentrations are somewhat higher than observed in ordinary chondrites. However, meteoritic metal typically contains Ni, Co, and P. Solubility experiments show that the presence of Ni, Co, P, and other elements decreases the solubility of C and N (e.g., see Wada et al., 1971). We therefore consider our solubility calculations
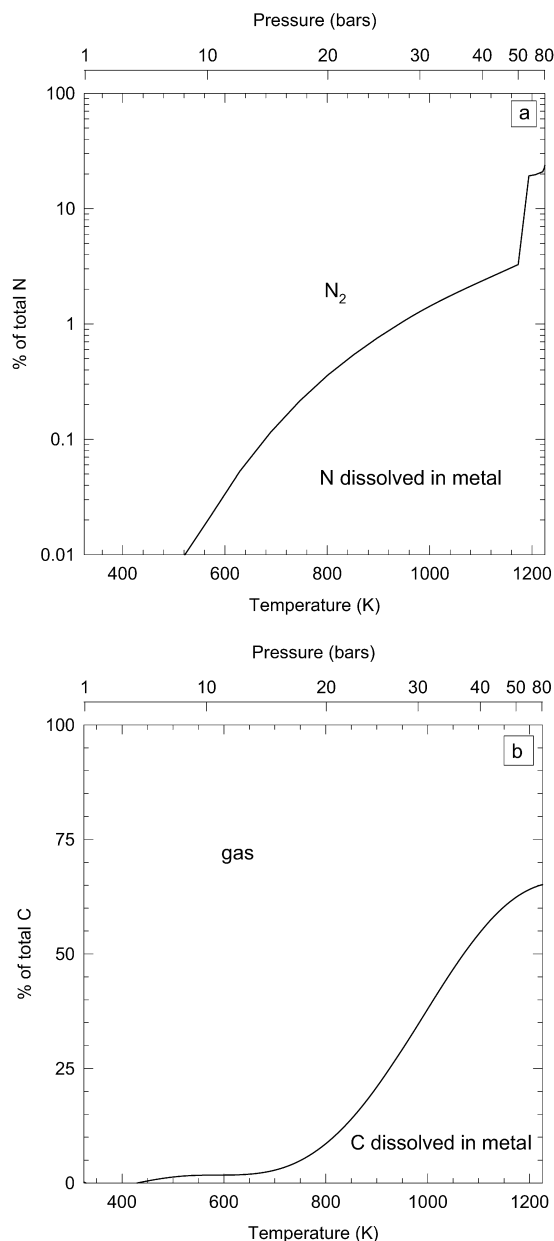
4. Discussion

We briefly discuss some of the applications of our results to outgassing on asteroids and the early Earth below.

4.1. Asteroidal outgassing and metamorphism of ordinary chondrites

The concept of meteorite metamorphism dates back at least as far as Merrill (1921). Dodd (1969) and McSween et al. (1988) reviewed metamorphism of the ordinary chondrites and emphasized several key points—metamorphism took place at temperatures of ~400–950 °C, pressures less than ~2000 bars, under dry conditions, was isochemical with respect to the major elements, and involved volatile element depletions with higher metamorphic grade. We used several of these conclusions as constraints on our calculations (e.g., temperature and pressure). However, we can also apply our results to questions such as the composition of metamorphic volatiles and the transport of volatile elements such as lead during metamorphism. We discuss the first topic below and are currently studying the latter topic, which is important for radiogenic dating of meteorites, to update our earlier work (Fegley, 1990).

As our figures show, we predict that methane was the major carbon-bearing gas during thermal metamorphism of ordinary chondrites. However, in much of the asteroidal literature, CO is assumed to be the major carbon gas (e.g., Hashizume and Sugiura, 1998; Krot et al., 1997; Wasson et al., 1993; Lee et al., 1992; Dodd, 1969; Mueller, 1964). The choice of CO gas may seem to be supported by heating experiments on chondrites, which typically produce much more CO than methane (e.g., Muenow et al., 1995). However, most of these experiments are done at very low pressures where CO would be the major C-bearing gas at equilibrium (see Fig. 7a). For example, Muenow et al. (1995) heated several H and L chondrites in vacuum at ~10^{-10} bars. As we verified for ourselves, this pressure is inside the CO stability field, but it is off scale to the right side of Fig. 7a. However, for the pressures that should exist within a meteorite parent body, methane clearly predominates.

The myth that CO is the major C-bearing gas during meteorite metamorphism apparently dates back to Mueller (1964). However, his calculations only show the ratios of different gas pairs (e.g., CO/CO_2, H_2/H_2O) and are not complete chemical equilibrium calculations that simultaneously consider the dual constraints of mass balance and chemical equilibrium. Furthermore, he never computed CH_4/CO ratios! As far as we can tell, the study by Bukvic (1979) was the first time anyone computed gas chemistry considering mass balance and chemical equilibrium at T–P conditions like those for ordinary chondrite metamorphism.

4.2. Planetary outgassing

A major impetus for this work was a desire to understand the nature of outgassed planetary atmospheres, particularly that of the Earth. The terrestrial atmosphere is believed to be a product of outgassing of volatile-bearing material during and/or

Fig. 17. (a) The chemical equilibrium distribution of nitrogen between gas and metal in average H-chondritic material plotted versus temperature. (b) The chemical equilibrium distribution of carbon between gas and metal in average H-chondritic material plotted versus temperature. Both calculations use the Hebe 3.7 Ma thermal profile.

to be an upper limit on the amount of C dissolved in metal. We found that even with such large C concentrations in metal, there was no discernible effect on the calculated gas chemistry, i.e. the major volatiles are still H_2 and CH_4 despite the large amount of C in metal. This is in stark contrast to the results of Hashizume and Sugiura (1998), who found that CO was the primary C-bearing gas, and CH_4 was never abundant. However, after reading a preprint of this paper, Professor Sugiura discovered that Hashizume and Sugiura (1998) used incorrect Gibbs energy data for methane. When this mistake was corrected he also found that CH_4 is the major C-bearing gas, in agreement with our results.

after the Earth's accretion (see e.g., Lange and Ahrens, 1982; Lewis and Prinn, 1984; Abe and Matsui, 1985; Prinn and Fegley, 1987; Kasting et al., 1993). However, the composition of the Earth's early atmosphere is controversial.

In the 1950s experiments by Stanley Miller and Harold Urey generated amino acids, carboxylic acids, hydrogen cyanide, and many other organic compounds by sparking a mixture of CH_4, H_2, H_2O, and NH_3 (Miller, 1955; Miller and Urey, 1959). Miller and Urey chose this reducing atmosphere because observations of Jupiter and Saturn showed that they contained ammonia and methane. Large amounts of H_2 were inferred to be present on Jupiter and Saturn. The gas giant planet atmospheres were regarded as captured remnants of the solar nebula and the atmospheres of the early terrestrial planets were assumed by analogy to have been similar (e.g., Oparin, 1953). Other scientists subsequently did many related experiments using electrical discharges, heat, or UV light applied to reducing gas mixtures (e.g., see Oró et al., 1990, and references therein). Miller–Urey reactions work best in $H_2 + CH_4$-bearing atmospheres, are still viable in mildly reducing atmospheres of $H_2 + CO$, but significantly less efficient in atmospheres of $H_2O + CO_2$ (Stribling and Miller, 1987).

However, atmospheric photochemists discovered that a reducing atmosphere of CH_4 and NH_3 was extremely vulnerable to destruction by UV sunlight (Kuhn and Atreya, 1979; Kasting et al., 1983). Since the Sun's UV flux was higher in the past, it was believed that such an atmosphere could not exist for a sufficient length of time to support the origin of life. This was especially true because, before the rise of methanogenic bacteria, there was no known mechanism capable of generating large amounts of CH_4.

Research done in the 1980s and 1990s suggested that the Earth's early atmospheric composition must have been more oxidizing. Impact degassing of comets (Ahrens et al., 1989; Abe and Matsui, 1985; Lange and Ahrens, 1982) releases primarily $H_2O + CO_2$, although recent work suggests that significant amounts of CH_4 may also be produced during impact degassing (Kress and McKay, 2004). Work on the oxidation state of the mantle suggests that it has not changed significantly over time (since ~3900 Ma), which means that volcanic gases during the past were oxidizing, similar to those of the present ($H_2O + CO_2$) (Delano, 2001). All of these discoveries and lack of a source of reducing gases suggested that the earliest atmosphere must have been oxidizing ($H_2O + CO_2$), or at least neutral ($H_2 + CO$), but definitely not reducing ($H_2 + CH_4$).

However the work by Bukvic (1979) and our results imply that Earth's early atmosphere was reducing. As mentioned earlier, Bukvic (1979) used a mixture of ~90% H and 10% CI chondrites to model volatile outgassing on the early Earth. He calculated the gas equilibrium composition within each layer of the planet's interior. Bukvic used a volcanic outgassing scenario, assuming that the gas moved from depth to the surface without interacting or equilibrating with the intervening layers, to predict the composition of the initial atmosphere. He found that the major outgassing products were N_2 at low temperatures and CH_4 and H_2 at higher temperatures. Fig. 18 shows our calculations for average H-chondritic material along the
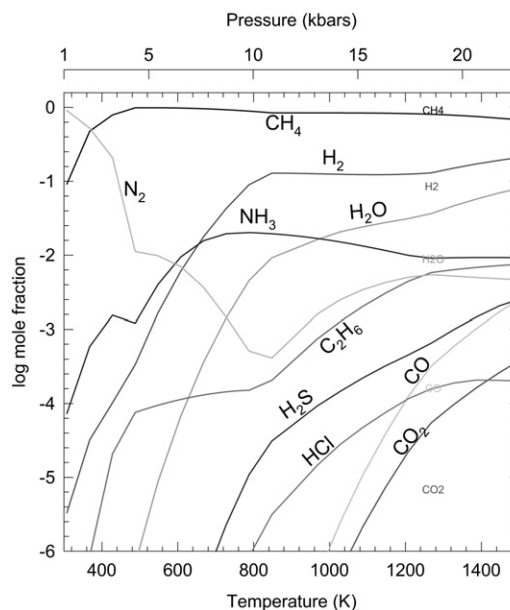

Fig. 18. Equilibrium gas chemistry as a function of temperature for average H-chondritic material for a terrestrial thermal profile.

terrestrial thermal profile used by Bukvic (1979). Our calculated compositions are nearly identical to his. Similar results were also obtained by Saxena and Fei (1988), who modeled mantle-fluid compositions for a chondritic system. Their results for $P = 10$ kbar, $T = 1273$ K for a carbonaceous chondrite are shown in Fig. 18 as small symbols and are very similar to our results. Saxena and Fei (1988) restricted their results to deep mantle conditions. However, we find that similar results hold at shallow depths as well.

Recent developments suggest that a reducing atmosphere is more stable than previously believed. Tian et al. (2005) found that hydrogen escape from the Earth's atmosphere was less efficient than previously believed. This allows an atmosphere with a large H/C ratio to be sustained much longer. Observations of Titan's atmosphere, which is composed primarily of CH_4 and N_2, show that photochemically produced hydrocarbon aerosols form a haze layer in the upper atmosphere that protects the lower atmosphere from photochemical destruction. Such a haze layer could also have been produced on the early Earth from outgassed methane and ammonia (Zahnle, 1986; Sagan and Chyba, 1997; Pavlov et al., 2000). The reduced rate of hydrogen loss coupled with a UV-shield of organic haze particles could have protected our predicted $CH_4 + H_2$ atmosphere from rapid destruction. However, detailed study of volatile outgassing on the early Earth and the fate of the outgassed atmosphere is beyond the scope of this paper and has to be pursued elsewhere.

5. Summary

We modeled outgassing of ordinary chondritic material in meteorite parent body and planetary settings. We found that for all three types of ordinary chondritic material (H, L, LL), the primary outgassed volatiles are CH_4 and H_2 gases. This

holds true over a wide range of temperatures and pressures, and for variable volatile abundances. We found that the gas equilibrium composition was relatively insensitive to variations in temperature, pressure, volatile element abundances, and dissolution of C and N in iron metal. To first-order, an open system favored highly reduced gases H_2, CH_4, and NH_3 throughout the planetesimal. For a terrestrial planetary setting, we found that gases remained highly reducing, with CH_4 being the favored product. Our predicted atmospheric composition favors the Miller–Urey synthesis of organic compounds, which may have significant implications for the origin of life on Earth.

Acknowledgments

Appendix A
List of solid phases included in our calculations

Element	NaCl	KNO_2	Phosphate/phosphide	$K_2Mg_2(SO_4)_3$
Al	$NiCl_2$	KNO_3	$Ca_5(PO_4)_3Cl$	$KAl(SO_4)_2$
C (diamond)	$TiCl_2$	$Mg(NO_3)_2$	$Ca_5(PO_4)_3F$	$KAl_3(OH)_6(SO_4)_2$
C (graphite)	$TiCl_3$	Mg_3N_2	$Ca_5(PO_4)_3(OH)$	$MgSO_4$
Ca	$TiCl_4$ (l)	$NaNO_2$	Fe_3P	$MnSO_4$
Co	**Fluoride**	$NaNO_3$	**Silicate**	Na_2SO_4
Cr	AlF_3	Si_3N_4	$Al_2Si_4O_{10}(OH)_2$	$NiSO_4$
Fe	CaF_2	Si_2N_2O	$Al_6Si_2O_{13}$	**Sulfide**
K	CoF_2	TiN	$Al_2Si_2O_5(OH)_4$	Al_2S_3
Mg	CoF_3	**Oxide**	$Ca_2Al_2Si_3O_{10}(OH)_2$	CaS
Mn	CrF_2	Al_2O_3	$Ca_2Al_2SiO_7$	Co_3S_4 (l)
Na	CrF_3	CaO	$Ca_2MgSi_2O_7$	Co_9S_8 (l)
Ni	FeF_2	$CaAl_{12}O_{19}$	$CaAl_2Si_2O_8$	CoS
P	FeF_3	$CaAl_4O_7$	$CaAl_4Si_2O_{10}(OH)_2$	CoS_2
S	KF	$CaTiO_3$	$CaFeSi_2O6$	CrS
Si	K_3AlF_6	CoO	$CaSiO_3$	$Fe_{0.875}S$
Ti	MgF_2	Co_3O_4	$Fe_7Si_8O_{22}(OH)_2$	FeS
Carbide	MnF_2	Cr_2O_3	Fe_2SiO_4	FeS_2
Al_4C_3	MnF_3	$Fe_{0.947}O$	$FeSiO_3$	K_2S
$Cr_{23}C_6$	MnF_4	Fe_3O_4	$KAl_3Si_3O_{10}(OH)_2$	MgS
Cr_3C_2	NaF	Fe_2O_3	$KAlSi_3O_8$	MnS
Cr_7C_3	Na_3AlF_6	FeO	$K_2Si_2O_4$	MnS_2
Fe_3C	$Na_5Al_3F_{14}$	$FeCr_2O_4$	K_2SiO_3	Na_2S
Fe_2C	NiF_2	$FeTiO_3$	Mg_2SiO_4	Ni_3S_2
$Mn_{15}C_4$	TiF_2	H_2O	$Mg_3Si_2O_5(OH)_4$	NiS
$Mn_{23}C_6$	TiF_3	H_2O_2	$Mg_3Si_4O_{10}(OH)_2$	NiS_2
Mn_3C	TiF_4	K_2O	$Mg_7Si_8O_{22}(OH)_2$	SiS
Mn_5C_3	**Hydride**	K_2O_2	$MgCaSi_2O_6$	SiS_2
Mn_7C_3	AlH_3	KO_2	$MgSiO_3$	TiS
SiC	CaH_2	$KAlO_2$	Mn_2SiO_4	TiS_2
TiC (l)	KH	MgO	$MnSiO_3$	
Carbonate	MgH_2	$MgAl_2O_4$	$Na_8Al_6Si_6O_{24}Cl_2$	
$CaCO_3$	NaH	Mn_2O_3	$NaAl_3Si_3O_{10}(OH)_2$	
$CaMg(CO_3)_2$	**Hydroxide**	Mn_2O_7 (l)	$NaFeSi_2O_6$	
$FeCO_3$	$Al(OH)_3$	Mn_3O_4	$NaAlSi_3O_8$	
K_2CO_3	$Ca(OH)_2$	MnO	$NaAlSiO_4$	
$MgCO_3$	$Co(OH)_2$	MnO_2	Na_2Si_2O5	
$MnCO_3$	$Fe(OH)_2$	Na_2O	Na_2SiO_3	
Na_2CO_3	$Fe(OH)_3$	Na_2O_2	**Silicide**	
$NaAlCO_3(OH)_2$	$FeOOH$	$NaAlO_2$	Cr_3Si	
Chloride	KOH	NaO_2	Cr_5Si_3	
$AlCl_3$	$Mg(OH)_2$	NiO	$CrSi$	
$CaCl_2$	$Mn(OH)_2$	SiO_2 (trid)	$CrSi_2$	
$CoCl_2$	$MnOOH$	SiO_2 (gl)	Ti_5Si_3	
$CrCl_2$	$NaOH$	SiO_2 (crist)	$TiSi$	
$CrCl_3$	$Ni(OH)_2$	SiO_2 (Qtz)	$TiSi_2$	
$FeCl_2$	$NiOOH$	Ti_2O_3	**Sulfate**	
$FeCl_3$	**Nitrite/nitrate**	Ti_3O_5	$Al_2(SO_4)_3$	
$FeOCl$	AlN	Ti_4O_7	$CaSO_4$	
KCl	CrN	TiO	$CaSO_4·2H_2O$	
$MgCl_2$	Cr_2N	TiO_2	$Fe_2(SO_4)_3$	
$MnCl_2$	Fe_4N		K_2SO_4	

References

Abe, Y., Matsui, T., 1985. The formation of an impact-generated H_2O atmosphere and its implications for the early thermal history of the Earth. J. Geophys. Res. 90 (Suppl.), C545–C559.

Ahrens, T.J., O'Keefe, J.D., Lange, M.A., 1989. Formation of atmospheres during accretion of the terrestrial planets. In: Atreya, S.K., Pollack, J.B., Matthews, M.S. (Eds.), Origin and Evolution of Planetary and Satellite Atmospheres. Univ. of Arizona Press, Tucson, pp. 328–385.

Alexander, C.M.O'D., Barber, D.J., Hutchison, R., 1989. The microstructure of Semarkona and Bishunpur. Geochim. Cosmochim. Acta 53, 3045–3057.

Allen Jr., R.O., Clark, P.J., 1977. Fluorine in meteorites. Geochim. Cosmochim. Acta 41, 581–585.

Ansdell, G., Dewar, J., 1886. On the gaseous constituents of meteorites. Proc. Roy. Soc. London 40, 549–559.

Aston, F.W., 1924. The rarity of the inert gases on the Earth. Nature 114, 786.

Barshay, S.S., 1981. Combined Condensation–Accretion Models of the Terrestrial Planets. Ph.D. thesis, MIT, Cambridge.

Belov, G.V., Iorish, V.S., Yungman, V.S., 1999. IVTANTHERMO for Windows—Database on thermodynamic properties and related software. CALPHAD 23, 173–180.

Brearley, A.J., 1997. Disordered biopyriboles, amphibole, and talc in the Allende meteorite: Nebular or parent body aqueous alteration? Science 276, 1103–1105.

Breger, I.A., Chandler, J.C., 1969. Determination of fixed water in rocks by infrared absorption. Anal. Chem. 41, 506–510.

Brett, R., Sato, M., 1984. Intrinsic oxygen fugacity measurements on seven chondrites, a pallasite, and a tektite and the redox state of meteorite parent bodies. Geochim. Cosmochim. Acta 48, 111–120.

Britt, D.T., Consolmagno, G.J., 2003. Stony meteorite porosities and densities: A review of the data through 2001. Meteor. Planet. Sci. 38, 1161–1180.

Brown, H., 1949. Rare gases and the formation of the Earth's atmosphere. In: Kuiper, G.P. (Ed.), The Atmospheres of the Earth and Planets. Univ. of Chicago Press, Chicago, pp. 260–268.

Bukvic, D.S., 1979. Outgassing of chondritic planets. M.S. thesis, MIT.

Chipman, J., 1972. Thermodynamics and phase diagram of the Fe–C system. Metall. Trans. 3, 55–64.

Chipman, J., Elliott, J.F., 1963. Physical chemistry of liquid steel. In: Sims, C.E. (Ed.), Electric Furnace Steelmaking, vol. 2. AIME, New York, pp. 95–179.

Consolgmano, G.J., Britt, D.T., Stoll, C.P., 1998. The porosities of ordinary chondrites: Models and interpretation. Meteor. Planet. Sci. 33, 1221–1229.

Craig, H., 1964. Petrological and compositional relationships in meteorites. In: Craig, H., Miller, S.L., Wasserburg, G.J. (Eds.), Isotopic and Cosmic Chemistry. North-Holland, Amsterdam, pp. 401–451.

Delano, J.W., 2001. Redox history of the Earth's interior since ~3900 Ma: Implications for prebiotic molecules. Origins Life 31, 311–341.

Dodd, R.T., 1969. Metamorphism of the ordinary chondrites: A review. Geochim. Cosmochim. Acta 33, 161–203.

Dreibus, G., Spettel, B., Wänke, H., 1979. Halogens in meteorites and their primordial abundances. In: Ahrens, L.H. (Ed.), Origin and Distribution of the Elements. Pergamon, New York, pp. 33–38.

Fegley Jr., B., 1983. Primordial retention of nitrogen by the terrestrial planets and meteorites. J. Geophys. Res. 88 (Suppl.), A853–A868.

Fegley Jr., B., 1990. Chondrite metamorphism: Models of volatile trace element transport. Meteoritics 25, 364.

Fegley Jr., B., Osborne, R., 2006. Practical chemical thermodynamics for geoscientists. Elsevier. In press.

Fegley Jr., B., Schaefer, L., 2006. Thermal outgassing of ordinary chondritic material. I. Nominal model results. Meteor. Planet. Sci. 41. Abstract A52.

Funkhouser, J., Jessberger, E., Müller, O., Zähringer, J., 1971. Active and inert gases released in Apollo 12 and Apollo 11 samples released by crushing at room temperature and by heating at low temperatures. Proc. Lunar Sci. Conf. 2, 1381–1396.

Gaffey, M.J., Gilbert, S.L., 1998. Asteroid 6 Hebe: The probable parent body of the H-type ordinary chondrites and the IIE iron meteorites. Meteor. Planet. Sci. 33, 1281–1295.

Garrison, D., Hamlin, S., Bogard, D., 2000. Chlorine abundances in meteorites. Meteor. Planet. Sci. 35, 419–429.

Ghosh, A., Weidenschilling, S.J., McSween Jr., H.Y., 2003. Importance of the accretion process in asteroid thermal evolution: 6 Hebe as an example. Meteor. Planet. Sci. 38, 711–724.

Gibson Jr., E.K., Bogard, D.D., 1978. Chemical alterations of the Holbrook chondrite resulting from terrestrial weathering. Meteoritics 13, 277–289.

Gibson Jr., E.K., Johnson, S.M., 1971. Thermal analysis—Inorganic gas release studies of lunar samples. Proc. Lunar Sci. Conf. 2, 1351–1366.

Gibson Jr., E.K., Moore, G.W., 1972a. Total nitrogen content of ordinary chondrites. Chemie der Erde 30, 115–131.

Gibson Jr., E.K., Moore, G.W., 1972b. Inorganic gas release and thermal analysis study of Apollo 14 and 15 soils. Proc. Lunar Sci. Conf. 2, 2029–2040.

Gooding, J.L., Muenow, D.W., 1977. Experimental vaporization of the Holbrook chondrite. Meteoritics 12, 401–408.

Grady, M., Wright, I.P., 2003. Elemental and isotopic abundances of carbon and nitrogen in meteorites. Space Sci. Rev. 106, 231–248.

Hart, S.R., Zindler, A., 1986. In search of a bulk Earth composition. Chem. Geol. 57, 247–267.

Hashizume, K., Sugiura, N., 1992. Various nitrogen isotopic compositions in H-chondrite metal. Meteoritics 27, 232.

Hashizume, K., Sugiura, N., 1995. Nitrogen isotopes in bulk ordinary chondrites. Geochim. Cosmochim. Acta 59, 4057–4069.

Hashizume, K., Sugiura, N., 1997. Isotopically anomalous nitrogen in H-chondrite metal. Geochim. Cosmochim. Acta 61, 859–872.

Hashizume, K., Sugiura, N., 1998. Transportation of gaseous elements and isotopes in a thermally evolving chondritic planetesimal. Meteor. Planet. Sci. 33, 1181–1195.

Hutchison, R., Alexander, C.M.O'D., Barber, D.J., 1987. The Semarkona meteorite: First recorded occurrence of smectite in an ordinary chondrite, and its implications. Geochim. Cosmochim. Acta 51, 1875–1882.

Jarosewich, E., 1990. Chemical analyses of meteorites: A compilation of stony and iron meteorite analyses. Meteoritics 25, 323–337.

Kaplan, I.R., 1971. Hydrogen. In: Mason, B. (Ed.), Handbook of Elemental Abundances in Meteorites. Gordon & Breach, New York, pp. 21–27.

Kargel, J.S., Lewis, J.S., 1993. The composition and early evolution of Earth. Icarus 105, 1–25.

Kasting, J.F., Zahnle, K.J., Walker, J.C.G., 1983. Photochemistry of methane in the Earth's early atmosphere. Precamb. Res. 20, 121–148.

Kasting, J.F., Eggler, D.H., Raeburn, S.P., 1993. Mantle redox evolution and the oxidation state of the Archean atmosphere. J. Geol. 101, 245–257.

Keller, L.P., 1998. A transmission electron microscope study of iron–nickel carbides in the matrix of the Semarkona unequilibrated ordinary chondrite. Meteor. Planet. Sci. 33, 913–919.

Koblitz, J., 2005. METBASE Version 7.1 for Windows.

Kothari, B.K., Goel, P.S., 1974. Total nitrogen in meteorites. Geochim. Cosmochim. Acta 38, 1493–1507.

Kress, M.E., McKay, C.P., 2004. Formation of methane in comet impacts: Implications for Earth, Mars, and Titan. Icarus 168, 475–483.

Krot, A.N., Zolensky, M.E., Wasson, J.T., Scott, E.R.D., Keil, K., Ohsumi, K., 1997. Carbide–magnetite assemblages in type-3 ordinary chondrites. Geochim. Cosmochim. Acta 61, 219–237.

Kuhn, W.R., Atreya, S.K., 1979. Ammonia photolysis and the greenhouse effect in the primordial atmosphere of the Earth. Icarus 37, 207–213.

Kung, C., Clayton, R.N., 1978. Nitrogen abundances and isotopic compositions in stony meteorites. Earth Planet. Sci. Lett. 38, 421–435.

Lange, M.A., Ahrens, T.J., 1982. The evolution of an impact-generated atmosphere. Icarus 51, 96–120.

Larimer, J.W., 1971. Composition of the Earth: Chondritic or achondritic. Geochim. Cosmochim. Acta 35, 769–786.

Lee, M.S., Rubin, A.E., Wasson, J.T., 1992. Origin of metallic Fe–Ni in Renazzo and related chondrites. Geochim. Cosmochim. Acta 56, 2521–2533.

Lewis, J.S., Prinn, R.G., 1984. Planets and Their Atmospheres: Origin and Evolution. Academic Press, New York.

Lodders, K., 2000. An oxygen isotope mixing model for the accretion and composition of rocky planets. Space Sci. Rev. 92, 341–354.

Lodders, K., Fegley Jr., B., 1997. An oxygen isotope model for the composition of Mars. Icarus 126, 373–394.

Mason, B., 1965. The chemical composition of olivine–bronzite and olivine-hypersthene chondrites. Am. Mus. Novit. 2223, 1–38.

Mason, B. (Ed.), 1971. Handbook of Elemental Abundances in Meteorites. Gordon and Breach, New York, 555 pp.

Mason, B., 1979. Data of Geochemistry, Chapter B: Cosmochemistry, Part 1. Meteorites. Geol. Surv. Prof. Pap. 440-B-1. GPO, Washington, DC, 132 pp.

Mason, B., Wiik, H.B., 1966. The composition of the Bath, Frankfort, Kakangari, Rose City, and Tadjera meteorites. Am. Mus. Novit. 2272, 1–24.

McNaughton, N.J., Borthwick, J., Fallick, A.E., Pillinger, C.T., 1981. Deuterium/hydrogen ratios in unequilibrated ordinary chondrites. Nature 294, 639–641.

McNaughton, N.J., Hinton, R.W., Pillinger, C.T., 1982. D/H ratios of some ordinary and carbonaceous chondrites. Meteoritics 17, 252.

McSween Jr., H.Y., Labotka, T.C., 1993. Oxidation during metamorphism of the ordinary chondrites. Geochim. Cosmochim. Acta 57, 1105–1114.

McSween Jr., H.Y., Sears, D.W.G., Dodd, R.T., 1988. Thermal metamorphism. In: Kerridge, J.F., Matthews, M.S. (Eds.), Meteorites and the Early Solar System. Univ. of Arizona Press, Tucson, pp. 102–113.

McSween Jr., H.Y., Bennett, M.E., Jarosewich, E., 1991. The mineralogy of ordinary chondrites and implications for asteroid spectrophotometry. Icarus 90, 107–116.

Menzies, O.N., Bland, P.A., Berry, F.J., Cressey, G., 2005. A Mossbauer spectroscopy and X-ray diffraction study of ordinary chondrites: Quantification of modal mineralogy and implications for redox conditions during metamorphism. Meteor. Planet. Sci. 40, 1023–1042.

Merrill, G.P., 1921. Metamorphism in meteorites. Geol. Soc. Am. Bull. 32, 395–416.

Merrill, G.P., 1926. Present condition of knowledge of the composition of meteorites. Proc. Am. Philos. Soc. 65, 119–130.

Michalak, G., 2001. Determination of asteroid masses. II. (6) Hebe, (10) Hygiea, (15) Eunomia, (52) Europa, (88) Thisbe, (444) Gyptis, (511) Davida and (704) Interamnia. Astron. Astrophys. 374, 703–711.

Miller, S.L., 1955. Production of some organic compounds under possible primitive Earth conditions. J. Am. Chem. Soc. 77, 2351–2361.

Miller, S.L., Urey, H.C., 1959. Organic compound synthesis on the primitive Earth. Science 130, 245–251.

Moore, C.B., Gibson, E.K., 1969. Nitrogen abundances in chondritic meteorites. Science 163, 174–176.

Mostefaoui, S., Zinner, E., Hoppe, P., Stadermann, F.J., El Goresy, A., 2005. In situ survey of graphite in unequilibrated chondrites: Morphologies, C, N, O, and H isotopic ratios. Meteor. Planet. Sci. 40, 721–743.

Mueller, R.F., 1964. Phase equilibria and the crystallization of chondritic meteorites. Geochim. Cosmochim. Acta 28, 189–207.

Muenow, D., Keil, K., McCoy, T.J., 1995. Volatiles in unequilibrated ordinary chondrites: Abundances, sources and implications for explosive volcanism on differentiated asteroids. Meteoritics 30, 639–645.

Müller, O., 1972. Chemically bound nitrogen abundances in lunar samples, and active gases release by heating at lower temperatures (250 to 500 °C). Proc. Lunar Sci. Conf. 2, 2059–2068.

Nash, L.K., Baxter, G.P., 1947. The determination of the gases in meteoritic and terrestrial irons and steels. J. Am. Chem. Soc. 69, 2534–2544.

O'Neill, H.St.C., 1987. Quartz–fayalite–iron and quartz–fayalite–magnetite equilibria and the free energy of formation of fayalite (Fe_2SiO_4) and magnetite (Fe_3O_4). Am. Miner. 72, 67–75.

Oparin, A.I., 1953. The Origin of Life. Dover, New York.

Oró, J., Miller, S.L., Lazcano, A., 1990. The origin and early evolution of life on Earth. Annu. Rev. Earth Planet. Sci. 18, 317–356.

Pavlov, A.A., Kasting, J.F., Brown, L.L., Rages, K.A., Freedman, R., 2000. Greenhouse warming by CH_4 in the atmosphere of the early Earth. J. Geophys. Res. 105, 11981–11990.

Prinn, R.G., Fegley Jr., B., 1987. The atmospheres of Venus, Earth, and Mars: A critical comparison. Ann. Rev. Earth Planet. Sci. 15, 171–212.

Ramdohr, P., 1973. The Opaque Minerals in Stony Meteorites. Elsevier, Amsterdam.

Richardson, F.D., 1953. The thermodynamics of metallurgical carbides and of carbon in iron. J. Iron Steel Inst. 175, 33–51.

Rietmeijer, F.J., Mackinnon, I.D.R., 1985. Layer silicates in a chondritic porous interplanetary dust particle. J. Geophys. Res. 90 (Suppl.), D149–D155.

Robert, F., Merlivat, L., Javoy, M., 1979. Deuterium concentration in the early Solar System: A hydrogen and oxygen isotopic study. Nature 282, 785–789.

Robert, F., Javoy, M., Halbout, J., Dimon, B., Merlivat, L., 1987a. Hydrogen isotope abundances in the Solar System. Part I. Unequilibrated ordinary chondrites. Geochim. Cosmochim. Acta 51, 1787–1805.

Robert, F., Javoy, M., Halbout, J., Dimon, B., Merlivat, L., 1987b. Hydrogen isotope abundances in the Solar System. Part II. Meteorites with terrestrial-like D/H ratio. Geochim. Cosmochim. Acta 51, 1807–1822.

Robie, R.A., Hemingway, B.S., 1995. Thermodynamic properties of minerals and related substances at 298.15 K and 1 bar (105 Pascals) pressure and at higher temperatures. US Geol. Survey Bull. 2131, 461 pp.

Rubin, A.E., 1997. Mineralogy of meteorite groups. Meteor. Planet Sci. 32, 231–247.

Rubin, A.E., Zolensky, M.E., Bodnar, R.J., 2002. The halite-bearing Zag and Monahans (1998) meteorite breccias: Shock metamorphism, thermal metamorphism and aqueous alteration on the H chondrite parent body. Meteor. Planet. Sci. 37, 125–141.

Russell, H.N., Menzel, D.H., 1933. The terrestrial abundance of the permanent gases. Proc. Natl. Acad. Sci. USA 19, 997–1001.

Sagan, C., Chyba, C., 1997. The early faint sun paradox: Organic shielding of ultraviolet-labile greenhouse gases. Science 276, 1217–1221.

Saxena, S.K., Fei, Y., 1988. Phase equilibrium in as system of chondritic composition: Implications for early mantle-fluid compositions. J. Geol. 96, 601–607.

Schaefer, L., Fegley Jr., B., 2004. A thermodynamic model of high temperature lava vaporization on Io. Icarus 169, 216–241.

Schaefer, L., Fegley Jr., B., 2005a. Alkali and halogen chemistry in volcanic gases on Io. Icarus 173, 454–468.

Schaefer, L., Fegley Jr., B., 2005b. Silicon tetrafluoride on Io. Icarus 179, 252–258.

Schaefer, L., Fegley Jr., B., 2005c. A reducing atmosphere from outgassing of the early Earth. Bull. Am. Astron. Soc. 37, 676. Abstract.

Schaefer, L., Fegley Jr., B., 2006. Thermal outgassing of ordinary chondritic material. II. Sensitivity studies. Meteor. Planet. Sci. 41. Abstract A158.

Slater-Reynolds, V., McSween Jr., H.Y., 2005. Peak metamorphic temperatures in type 6 ordinary chondrites: An evaluation of pyroxene and plagioclase geothermometry. Meteor. Planet. Sci. 40, 745–754.

Spear, F.S., 1995. Metamorphic Phase Equilibria and Pressure–Temperature–Time Paths. Mineral. Soc. Am., Washington, DC. 799 pp.

Stribling, R., Miller, S.L., 1987. Energy yields for hydrogen cyanide and formaldehyde syntheses: The HCN and amino acid concentrations in the primitive ocean. Origins Life 17, 261–273.

Sugiura, N., Kiyota, K., Zashu, S., 1996. Nitrogen isotopic compositions of some solar-gas-rich chondrites. In: Proc. NIPR Symp. Antarct. Meteorites, No. 9, pp. 189–207.

Sugiura, N., Kiyota, K., Hashizume, K., 1998. Nitrogen components in primitive ordinary chondrites. Meteor. Planet. Sci. 33, 463–482.

Takahashi, E., 1983. Melting of a Yamato L3 chondrite (Y-74191) up to 30 kbar. In: Proc. Symp. Antarct. Meteorites, vol. 8, pp. 168–180.

Tian, F., Toon, O.B., Pavlov, A.A., De Sterk, H., 2005. A hydrogen-rich early Earth atmosphere. Science 308, 1014–1017.

Travers, M.W., 1898, 1899. The origin of the gases evolved on heating mineral substances, meteorites, etc. Proc. Roy. Soc. London 64, 130–142.

Urey, H.C., Craig, H., 1953. The composition of the stone meteorites and the origin of the meteorites. Geochim. Cosmochim. Acta 4, 36–82.

Van Zeggern, F., Storey, S.H., 1970. The Computation of Chemical Equilibria. Cambridge Univ. Press, London, UK.

Vdovykin, G.P., Moore, C.B., 1971. Carbon. In: Mason, B. (Ed.), Handbook of Elemental Abundances in Meteorites. Gordon & Breach, New York, pp. 81–91.

Von Seckendorff, V., O'Neill, H.St.C., 1993. An experimental study of Fe–Mg partitioning between olivine and orthopyroxene at 1173, 1273, and 1473 K and 1.6 GPa. Contrib. Mineral. Petrol. 113, 196–207.

Wada, T., Wada, H., Elliott, J.G., Chipman, J., 1971. Thermodynamics of the Fcc Fe–Ni–C and Ni–C alloys. Metall. Trans. 2, 2199–2208.

Walter, L.S., Doan, A.S., 1969. Determination of oxygen activities of chondritic meteorites. Geol. Soc. Am. Abstracts Prog. 1, 232–233.

Wänke, H., 1981. Constitution of the terrestrial planets. Philos. Trans. R. Soc. London A 303, 287–302.

Wasson, J.T., Rubin, A.E., Kallemeyn, G.W., 1993. Reduction during metamorphism of four ordinary chondrites. Geochim. Cosmochim. Acta 57, 1867–1878.

Williams, R.J., 1971. Equilibrium temperatures, pressures, and oxygen fugacities of the equilibrated chondrites. Geochim. Cosmochim. Acta 35, 407–411.

Wilson, L., Keil, K., Browning, L.B., Krot, A.N., Bourcier, W., 1999. Early aqueous alteration, explosive disruption, and reprocessing of asteroids. Meteor. Planet. Sci. 34, 541–557.

Yang, J., Epstein, S., 1983. Interstellar organic matter in meteorites. Geochim. Cosmochim. Acta 47, 2199–2216.

Zahnle, K.J., 1986. Photochemistry of methane and the formation of hydrocyanic acid (HCN) in the Earth's early atmosphere. J. Geophys. Res. 91, 2819–2834.